Title: Manipulating condensation of thermo-sensitive SUF4 protein tunes flowering time in Arabidopsis thaliana

Authors: Heather M. Meyer[1*], Takashi Hotta[2,3], Andrey Malkovskiy[1], Yixian Zheng[2], and David W. Ehrhardt[1*]

Affiliations:
1. Department of Plant Biology, Carnegie Institution for Science, Stanford, CA 94305, USA.

2. Department of Embryology, Carnegie Institution for Science, 3520 San Martin Dr. Baltimore, MD 21218, USA.

3. Department of Cell and Developmental Biology, University of Michigan, Ann Arbor, 109 Zina Pitcher Pl. Ann Arbor MI 48109, USA

* Corresponding authors: Heather M. Meyer:hmeyer@ciw.edu, David W. Ehrhardt: ehrhardt@stanford.edu

Abstract (286 words): Intrinsically disordered proteins (IDP) lack stable tertiary structures, which allows them to change conformation and function under different physicochemical conditions. This may be highly advantageous for plants, which often use changes in their environment to elicit a variety of responses, including developmental events. For instance, some plants delay flowering in the fall and require exposure to winter temperatures as a cue to initiate flowering the following spring. Many of the genes involved in temperature-dependent flowering have been extensively studied in *Arabidopsis*, yet how plants coordinate their molecular states with seasonal temperature change is poorly understood. Here, we explore the role of temperature-sensitive phase separation of the IDP and flowering-time regulator, SUPPRESSOR OF FRIGIDA 4 (SUF4), in modulating flowering time. SUF4 has a well-defined role in regulating temperature-dependent flowering time by activating the master floral suppressor *FLOWERING LOCUS C (FLC)*. We show that in plant nuclei, SUF4 is a temperature-sensitive protein that assembles into biomolecular condensates in warm temperatures (20°C). When temperatures cool (4°C), SUF4 nuclear condensates disassemble, causing SUF4 to disperse within the nucleoplasm. Additionally, we demonstrate that the number of SUF4 condensates quantitatively correlates with flowering time. Progressive alterations to the amino acid composition of SUF4's disordered region cause likewise progressive changes in temperature-dependent condensation both *in vitro* and *in vivo*, *FLC* transcription, and the onset of flowering. Lastly, we observe that SUF4

condensates coincide with the accumulation of other key flowering-time proteins (FRIGIDA and ELF7). These findings indicate that condensation of SUF4 likely plays a pivotal role in promoting flowering, possibly by concentrating and stabilizing regulatory factors needed for the transcriptional activation of *FLC* through temperature-dependent phase separation. This research suggests that in plants, IDPs can sense environmental cues and regulate critical developmental processes.

One-Sentence Summary: Evidence suggest that *Arabidopsis* uses temperature-sensitive condensation to regulate *FLC* transcription and flowering time.

Main text:

INTRODUCTION:

The survival of all species depends on their ability to reproduce. For plants, reproductive success relies heavily on the onset of flowering, a phenological feature influenced by changes in seasons. Many plant species, including winter crops, have evolved to use long exposure to winter temperatures (e.g., vernalization) as a cue to flower in the following spring. Temperature-induced development plays a crucial role in the long-term reproductive success and yield of plants, enabling them to synchronize their flowering with seasonal pollinators and set seed during favorable climatic conditions. Thus, as climate change drives new spatial and seasonal temperature trends, it is increasingly important to understand how plants physically sense and integrate thermal shifts.

In the model plant *Arabidopsis thaliana*, temperature-dependent flowering is modulated by the epigenetic silencing of the *FLOWERING LOCUS C (FLC)*. *FLC* encodes a MADS-box transcription factor that represses flowering by silencing floral-inducing genes including *FT* and *SOC1*[1–3]. In warm temperatures, SUPPRESSOR OF FRIGIDA 4 (SUF4), FRIGIDA (FRI), and FRI-associated proteins transcriptionally activate *FLC* by recruiting chromatin modifiers, such as members of the PAF1 complex, which methylate histone H3 lysine 4 (H3K4me3) at *FLC*'s transcriptional start site [3,4]. Conversely, exposure to cold temperatures promotes antisense long non-coding RNAs and a second set of chromatin remodelers belonging to the POLYCOMB REPRESSIVE COMPLEX 2 (PRC2) to epigenetically silence *FLC*, ultimately priming plants to flower the following spring [5,6]. While many elements of the genetic and epigenetic regulation of temperature-dependent flowering are well established, the mechanisms by which plants sense and transduce thermal changes to elicit these responses remain a mystery.

79 Intrinsically disordered proteins (IDPs) are highly sensitive to changes in
80 their physical environment [7,8]. Unlike canonical proteins, which assume relatively
81 stable structures with limited conformational changes in response to different
82 stimuli and physiological conditions, IDPs possess low sequence complexity and a
83 reduced ability to form stable tertiary structures. This inherent flexibility enables
84 them to readily alter their conformation and function under varying physical and
85 solution conditions. For example, many IDPs undergo phase separation into liquid-
86 like protein droplets or viscoelastic hydrogels, facilitating rapid concentration,
87 formation, and/or stabilization of higher-order complexes in response to
88 environmental changes[8,9]. The ability for IDPs to phase separate has led to the
89 intriguing hypothesis that this mechanism could serve as a biological means for
90 cells and organisms to perceive and adapt to environmental signals[,10]. However,
91 verifying this hypothesis poses a challenge due to the difficulty of distinguishing
92 functions derived from phase separation from other protein properties.
93 Here, we identified that one of the key proteins required for regulation of
94 *FLC* transcription and temperature-dependent timing of flowering, SUPPRESSOR
95 OF FRIGIDA 4 (SUF4), exhibits significant similarities with BUGZ, an IDP
96 known for its temperature-dependent phase condensation and involvement in
97 mitotic chromosome alignment in animal cells[10–12]. Both proteins are comparable
98 in size and feature two highly conserved zinc finger domains at their N-termini,
99 followed by intrinsically disordered domains with low amino acid complexity
100 enriched in proline, valine, and glycine residues. Given these structural parallels,
101 along with BuGZ's documented biophysical behavior and SUF4's genetic and
102 molecular implications in flowering timing, we asked if SUF4 also undergoes
103 temperature-dependent phase transitions, using changes in its phase behavior to
104 regulate the seasonal onset of flowering time.
105 Using confocal microscopy, genetics, and biochemistry, we discovered that
106 SUF4 is indeed a temperature-sensitive protein that undergoes phase separation *in*
107 *vitro*, forming proteinaceous droplets, and *in planta*, promoting the formation of
108 nuclear condensates. At warm temperatures (20°C), SUF4 dynamically forms
109 nuclear condensates, whereas at low temperatures (4°C), these condensates fail to
110 form, causing SUF4 to disperse throughout the nucleoplasm. Furthermore, through
111 use of targeted mutagenesis, we established the significance of SUF4's disordered
112 region in nuclear condensate formation and the regulation of flowering time. Plants
113 expressing SUF4 variants with graded aromatic/hydrophobic-to-hydrophilic amino
114 acid substitutions in this region exhibit graded alterations in condensate formation,
115 *FLC* transcript levels, and flowering-time responses. To explore the relationship
116 between SUF4 condensates and other proteins involved in flowering time, we
117 labeled two significant *FLC* regulators, FRIDIGA (FRI), and the PAF1-complex
118 member EARLY FLOWERING 7 (ELF7) with fluorescent markers. We observed

that both proteins often appear in nuclear condensates that co-localize with a subset of SUF4 condensates, indicating that SUF4 condensation occurs where other important regulators of flowering time also accumulate. Interestingly, while FRI could assemble into condensates containing SUF4 in some tissues (lateral roots), its accumulation was apparently antagonized by SUF4 condensation in other tissue (primary roots). Our findings provide strong evidence supporting the hypothesis that SUF4 regulates flowering time by utilizing temperature-dependent phase separation, which likely functions to enhance the activity of regulatory factors, including itself, that are necessary for the transcriptional activation of *FLC*.

RESULTS:

SUF4 forms nuclear condensates *in planta.*

To investigate the hypothesis that SUF4 phase separation is important for the regulation of flowering time, we first needed to assess if SUF4 undergoes temperature-dependent condensation *in vivo*. To do this, we engineered a monomeric fluorescent mEGFP-SUF4 fusion protein expressed from the putative *SUF4* native promoter and 3' UTR (pSUF4::mEGFP-SUF4) and introduced this construct into *suf4* (*FRI*) mutant plants. We identified several transgenic lines that rescued both the early flowering phenotype of the null mutant and the transcriptional activity of *SUF4* as measured by the transcripts level of its downstream target *FLC* (Supplemental Fig. 1A and 1B), suggesting that the *SUF4* transgene is fully functional and expressed at adequate levels. We picked one of these lines to perform all subsequent analyses regarding SUF4.

To assess the subcellular localization and behavior of SUF4 within living plant cells, we imaged live cells using confocal microscopy at room temperature. In both the shoot and the root, we observed SUF4 to exhibit a diffuse localization pattern within the nucleoplasm and accumulate in nuclear foci reminiscent of biomolecular condensates (Supplemental Fig. 2). Additionally, we found that SUF4 localized in the nucleolar cavity, an elusive membrane-less compartment that forms within the nucleolus (Supplemental Fig. 2). The nucleolar cavity is a thermo-responsive structure in plant cells that exchanges its contents with the nucleus [13–15]. However, we directed our analysis toward the function of the nucleoplasmic foci outside of the nucleoli where most genes, such as *FLC*, are transcribed [16,17].

If SUF4 condensates function as thermosensors, their formation should exhibit temperature sensitivity across a physiologically relevant temperature range *in vivo*. To test this, we subjected SUF4 rescue plants to a 24-hour cold treatment at 4°C and then live imaged epidermal and cortical cells in the division and growth zones of primary roots as the plants rewarmed to 20°C. At the beginning of rewarming, mEGFP-SUF4 appeared diffuse and no condensates were detected

159 (Fig. 1A and 1B). As plants began to warm up, SUF4 signal progressively
160 partitioned into nuclear condensates, with condensates forming within seconds to
161 minutes once exposed to room temperature conditions. To ensure that these
162 changes were temperature-induced, we also imaged plants over the same time
163 course under constant 20˚C (Fig. 1B). Although some condensates showed
164 evidence of forming and dissipating over the time scale of observation (<10mins),
165 a portion of SUF4 always remained partitioned in condensates. Together, our
166 results suggest that SUF4 is a temperature-sensitive protein that assembles into
167 biomolecular condensates in warm temperatures and remains diffuse in the
168 nucleoplasm in cold temperatures.
169
170 **SUF4 phase separates *in vitro*.**
171 SUF4 is orthologous to the animal protein BuGZ (Supplemental Fig. 3), an
172 IDP initially found to undergo temperature-dependent phase separation *in vitro* and
173 regulate spindle assembly *in vivo*[10–12]. Therefore, to assess the potential for SUF4
174 to undergo phase separation independently of any plant cell factors, we expressed
175 and purified 6xHis-mVenus-SUF4 (isoform 1, WT) from SF9 insect cells. Using
176 both fluorescence and DIC microscopy, we observed that 6xHis-mVenus-SUF4
177 underwent phase separation at high temperatures (25μM at 37˚C) and remained
178 miscible at low temperatures (25μM at 4˚C) when suspended in physiologically
179 relevant buffers (Fig. 2A, Supplemental Fig. 4, see methods). These results suggest
180 that, similar to BuGZ, SUF4 is a phase-separating protein displaying low critical
181 solution temperature (LCST) behavior. To investigate further the phase behavior of
182 SUF4, we conducted a turbidity assay to determine the thermal setpoint required
183 for SUF4's condensation. We found that 25μM of 6xHis-mVenus-SUF4 was fully
184 miscible between 4-10˚C but became increasingly turbid as temperatures gradually
185 rose to 30˚C (Fig. 2B). Additionally, in line with other phase-separating proteins,
186 SUF4's phase transition is concentration-dependent, with lower concentrations of
187 SUF4 requiring higher temperature regimes to undergo phase separation (Fig. 2B,
188 Supplemental Fig. 4). These results indicate that, similar to BuGZ, SUF4 is a
189 temperature-sensitive protein that undergoes LCST phase separation *in vitro*.
190
191 **SUF4's disordered region drives nuclear condensate formation *in vitro* and *in***
192 ***planta.***
193 IDP phase separation is driven by multivalent interactions, such as those
194 facilitated by aromatic/hydrophobic residues like tyrosine and phenylalanine.
195 Moreover, these same residues are required for *in vitro* condensation of SUF4's
196 ortholog, BuGZ[11,12]. Despite being a proline-rich protein, SUF4 contains a total of
197 14 regularly spaced tyrosine and phenylalanine residues within its disordered
198 region, with two of these residues falling in putative splice sites (Supplemental Fig.

199 3). To test if aromatic/hydrophobic residues in SUF4's disorder region promote its
200 temperature-dependent condensation, we created a SUF4 variant, termed 12S
201 SUF4, in which we substituted 12 non-splice-interfering tyrosine and
202 phenylalanine residues with serine and asked if this variant had a different phase
203 separation thermal setpoint *in vitro*. We found 12S SUF4 had a large shift in its
204 thermosensitive capabilities to phase separate, such that 25µM of purified 12S
205 SUF4 now required temperatures nearing 50˚C to begin phase separating as
206 opposed to 20˚C for the native protein (Fig. 2B). These results suggest that
207 changing SUF4's aromatic/hydrophobic patterning is sufficient to disrupt
208 condensate formation *in vitro* by increasing the thermal set point at which SUF4
209 can phase separate.
210 To test if changes in SUF4 aromatic/hydrophobic patterning also influenced
211 condensate formation *in vivo*, we generated the same 12 mutations in the mEGFP-
212 SUF4 fusion protein expressed over a chromosomal null locus (pSUF4::mEGFP-
213 12S SUF4). Similar to our observations *in vitro,* we found that 12S SUF4 exhibited
214 a severe reduction in condensate formation *in vivo*. On average, 12S SUF4 plants
215 formed 0-1 nuclear condensates per nucleus in root epidermal and cortical nuclei at
216 20˚C, as compared to 4-5 per nucleus formed in rescue SUF4 (Fig. 3A and 3B,
217 nuclei observed: 12S SUF4 n= 27, rescue SUF4 n=32). These results suggest that
218 the altered coacervation properties of 12S SUF4 are maintained in the complex
219 environment of the living cell.
220 Next, we investigated if SUF4 uses phase separation as a means to regulate
221 flowering time. As a first step in testing this hypothesis, we asked if 12S SUF4
222 variant plants displayed a phenotypic difference in its response as compared to the
223 rescue SUF4 plants. Using a leaf counting assay, we found that 12S SUF4 plants
224 transitioned to flowering much sooner, producing significantly fewer rosette leaves
225 before flowering (Long Day (LD): 35 leaves (n=30)) as compared to SUF4 rescue
226 plants (LD: 71 leaves (n=29)), but significantly more so than the *suf4* null mutant
227 (LD: 26 leaves (n=31)) (Fig. 2C-E, Supplemental Fig. 5). Previous research has
228 shown that high levels of *FLC* must be produced for the suppression of flowering
229 time. We therefore asked if the flowering time phenotype caused by the 12S
230 mutant protein was correlated with a reduction in *FLC* transcripts. We found plants
231 expressing the 12S variant to produce approximately 18-fold fewer *FLC* transcripts
232 than our SUF4 rescue lines but 2-fold more than *suf4* null mutants (Fig. 3C). Thus,
233 although *FLC* still undergoes some transcription in the 12S SUF4 variant, the
234 mutations that caused disruption of SUF4 temperature-sensitive condensation
235 greatly accelerated the onset of flowering.
236
237 **Tuning SUF4 phase behavior causes graded changes in *FLC* transcription and**
238 **flowering time**

239 Previous work from Jiang et al (2015) has shown that the *in vitro* phase
240 behavior of SUF4's ortholog, BuGZ, may be tuned by incrementally decreasing the
241 number of combined phenylalanine and tyrosine to serine substitutions[10]. This
242 finding, paired with the correlation between SUF4 phase separation and flowering
243 time, prompted us to further assess if SUF4's phase change properties themselves
244 were critical for dictating different flowering time outcomes. We reasoned that if
245 so, substituting a smaller number of the phenylalanine and tyrosine residues should
246 lead to a scalable intermediate phase separation phenotype and proportionally tune
247 flowering time outcomes via decreasing the transcriptional levels of *FLC*. To test
248 this prediction, we created an intermediate SUF4 variant that only had 5 combined
249 tyrosine and phenylalanine to serine substitutions termed, 5S SUF4, and assessed
250 its phase separating thermal setpoint *in vitro*. Consistent with what had been
251 observed for BuGZ, we found purified 5S SUF4 to have a thermal shift that ranges
252 between the phase change of rescue SUF4 and 12S SUF4 *in vitro* (Fig. 2B; 25µM
253 showed a steep phase transition at 40˚ C instead of 20˚C like rescue SUF4 and
254 50˚C like 12S SUF4).
255 To test the function of the 5S SUF4 variant *in vivo*, we introduced it into
256 *suf4* null mutant plants and asked if these plants exhibited intermediate phenotypes
257 relating to SUF4 phase separation, *FLC* transcriptional output, and flowering time.
258 Remarkably, we found 5S SUF4 plants to display an intermediate condensate
259 phenotype *in vivo*, in which they formed significantly fewer nuclear condensates in
260 root epidermal and cortical cells than rescue SUF4 but more than 12S SUF4 (Fig.
261 3A and 3B; rescue SUF4:4-5, 5S SUF4:2-3, 12S SUF4:0-1). This outcome differed
262 from the results observed with 5S SUF4 purified protein, which showed no phase
263 separation at room temperature, suggesting that the complex cellular environment
264 may influence the phase behavior of 5S SUF4 (Figure 2A). Moreover, 5S SUF4
265 plants exhibited *FLC* transcript levels and flowering time responses that both fell
266 between rescue SUF4 and 12S (Fig. 3C-E, Supplemental Fig. 5; rescue SUF4
267 produced 20-fold/ LD: 71 leaves (n=29), 5S SUF4: 10-fold/LD: 43 leaves (n=39),
268 12S SUF4 3-fold/ LD: 35 leaves (n=30)). These results indicate that tuning the
269 LCST behavior of SUF4 is sufficient to predictably change the onset of flowering
270 through modulating transcript levels of *FLC*.
271
272 **SUF4's exchange dynamics scale with changes in LCST behavior**
273 Biomolecular condensates may assume a broad range of material properties,
274 spanning liquid-, gel-, or solid-like structures, with these respective properties
275 often being hypothesized as being important for their biological function[7,18–20].
276 Under *in vitro* conditions, purified and condensed SUF4 exhibited behavior
277 consistent with a liquid, similar to its ortholog BuGZ. For example, *in vitro*
278 condensates on glass assume a round outline, as expected at a liquid-liquid

interface, and are rapidly and repeatedly reversible with temperature change (Fig. 2A, Supplemental Fig. 4). However, whether SUF4's material properties remain liquid-like during interactions with other biomolecules under native cellular conditions remains unknown. Previous research has suggested that the exchange dynamics of molecules within condensates are expected to correlate with their material state, with faster exchange rates in liquid-like condensates and slower rates in more solid-like structures[20,21]. Thus, to investigate the exchange dynamics of SUF4 and whether these dynamics are affected in our SUF4 variants, we conducted fluorescence recovery after photobleaching (FRAP) experiments on rescue SUF4, 5S SUF4, and a hydrophobic variant termed 30I SUF4, which contains 30 alanine-to-isoleucine substitutions in its disordered region (Supplemental Fig. 6). We excluded the 12S SUF4 variant as it rarely formed condensates. FRAP was performed in a small region of approximately 1.094 microns^2, centered on a prominent mEGFP-SUF4 nuclear body in each cell assayed. Our findings revealed that changing the hydrophobicity of SUF4 greatly affected its FRAP dynamics. 30I SUF4 condensates did not reach their half recovery time within a 10-minute period, whereas both rescue SUF4 and 5S SUF4 rapidly reached their half recovery time within seconds (Fig. 4A, rescue SUF4: t1/2=1.27 seconds, n=13; 5S SUF4 t1/2=0.85 seconds, n=12, 1-sided t-test $p<0.01$). Additionally, 30I SUF4 condensates exhibited a higher "immobile" fraction compared to SUF4 rescue and 5S SUF4, which both largely recovered (30I SUF4 = 0.094 mobile fraction, SUF4 rescue = 0.85 mobile fraction, and 5S SUF4 = 0.76 mobile fraction; Fig 4A). Interestingly, despite 30I SUF4 having formed many condensates that were relatively slow to recover, we did not observe any rescue in plant phenotype concerning *FLC* transcription or flowering time (Supplemental Fig. 6). Previous studies have suggested that the biophysical properties of some condensates must fall within a fluidic window, in which being overly solid or fluid-like can lead to a decrease in functionality [20–25]. Therefore, in agreement with these findings, we propose that SUF4 needs to maintain a specific state of fluidity in order to function optimally.

A notable finding from our FRAP experiments is that the recovery curves of 5S SUF4 signal exhibited a lower R^2 value on average when fitted to a single exponential recovery model, along with a lower bleaching depth compared to those observed in our rescue lines (rescue SUF4 $R^2 = .73$, 5S SUF4 $R^2 = .53$). This observation prompted us to further investigate the behavior of condensates in this background. In doing so, we noticed that 5S SUF4 condensates appeared to display greater motility compared to rescue SUF4 condensates. An increase in particle motility could explain the reduced model fit as movement of condensates out of the focal plane would tend to reduce their brightness, thus affecting measurement of signal recovery kinetics. To quantify the perceived difference in motility, we

319 measured the total distance traveled by each condensate during our FRAP analysis.
320 On average, we found that 5S SUF4 condensates traveled significantly greater
321 distances within the nucleoplasm compared to rescue SUF4 condensates (Fig. 4B,
322 average distance of 1.802 microns for rescue SUF4 and 3.046 microns for 5S
323 SUF4). These results indicate that 5S SUF4 condensates are less constrained in
324 their positional behavior compared to their rescue SUF4 counterparts.
325
326 **SUF4 colocalizes with FRI within nuclear condensates at room temperature in**
327 **root cells recently derived from meristems**
328 SUF4 has been shown previously to physically and genetically interact with
329 FRIGIDA (FRI) and other members of the vernalization pathway, and this
330 complex has been proposed to transcriptionally activate *FLC* [3,4]. Therefore, to ask
331 if SUF4 condensation occurs where other flowering time regulators are present,
332 and to explore the possibility that SUF4 condensation might function to regulate
333 *FLC* by concentrating flowering time proteins, we tested if there was an observable
334 spatial relationship between SUF4 and FRI *in vivo*. We generated a fluorescently-
335 labeled FRI fusion gene (FRI-mScarletI) that expresses from the native upstream
336 sequence of FRI (pFRI) and transformed it into a mEGFP-SUF4 rescue line. Under
337 room temperature conditions, we found FRI-mScarletI to exist in one of two
338 distinct phase states within the nucleoplasm of root epidermal and cortical cells
339 within the division and growth zones— either uncondensed and diffuse within the
340 nucleoplasm or assembled into one-to-two apparent condensates (Fig 5A and B).
341 Next, we tested if FRI-mScarletI condensates colocalized with mEGFP-
342 SUF4 condensates. To measure co-localization, we considered condensates to be
343 colocalized if the centroids of spot-detected condensates were closer together than
344 the radius of the kernel used to detect the SUF4 condensates (<250nm). Out of 56
345 FRI-mScarletI condensates analyzed, 38 of them co-localized with a SUF4
346 condensate (Fig. 5A; 68% co-localization, n=47 nuclei, distance threshold=0.3µm).
347 To ask whether this degree of colocalization was specific to the vernalization
348 complex and not likely due to chance alone given the density of SUF4 nuclear
349 condensates, we co-transformed the nuclear splicing speckle marker U2B”-mRFP
350 into mEGFP-SUF4 rescue plants, a marker, like that for FRI, produces 1-2 bodies
351 of larger size per nucleus. In the 18 nuclei examined, we found no instances of
352 U2B" bodies co-localizing with SUF4 at room temperature conditions (0/19 U2B”
353 speckles; Fig. 5A). These data demonstrate a remarkable degree of colocalization
354 between SUF4 and FRI, suggest that the formation of FRI condensates under warm
355 temperatures is not a random occurrence but rather occurs preferentially where
356 condensation of SUF4 also occurs.
357
358 **SUF4 and FRI colocalization depends on tissue type and temperature**

359 FRI has recently been reported to have no quantifiable physical interactions
360 with SUF4 and to accumulate into nuclear condensates when exposed to extended
361 periods of low temperatures [26–28]. Thus, to test the spatial relationship between
362 SUF4 and FRI in the cold, we exposed mEGFP-SUF4 and FRI-mScarletI co-
363 expressing plants to 4˚C for 24 hours and imaged their root cells as the plants
364 warmed up. Consistent with previous findings[26–28], we found FRI to form cold-
365 induced nuclear condensates. However, unlike the case at room temperature
366 (~21˚C), these condensates did not co-localize with SUF4. Instead, SUF4
367 condensates would sometimes appear in the same locations where FRI condensates
368 previously existed as plants began to warm (observed in at least 7 nuclei; Fig 6A
369 and B). These results suggest an antagonistic or independent relationship between
370 cold-induced FRI condensates and SUF4. Additionally, they suggest that FRI
371 undergoes cold-induced phase separation that is independent of *FLC* activation (a
372 process reliant on SUF4).
373 Given the established relationship between the spatiotemporal organization
374 of proteins and their biological function, we investigated the root tissue types in
375 which both warm- and cold-induced FRI condensation occurred. Under warm
376 temperatures, we observed the presence of FRI condensates in the division and
377 growth zones of a subset of emerging and young lateral roots but not in primary
378 roots (Fig. 6C, Nplants=8/29 lateral roots, Nplants=0/34 primary roots of 6-13
379 DAG). This was different to what occurred under cold temperatures, in which we
380 found FRI condensing in all root types, including the primary roots (Supplemental
381 Fig. 7). Interestingly, the occurrence of warm-induced FRI condensates within a
382 given lateral root cell was highly variable among lateral roots, with detectable FRI-
383 mScarletI condensates found in anywhere from 30% to 94% of the epidermal and
384 cortical cells within the growth zone (Supplemental Fig. 7). The seemingly
385 stochastic patterns of nuclei containing FRI condensates among and within lateral
386 meristems resemble the previously described phenomenon of transcriptional and
387 translational "bursting," which has been associated with epigenetic and phenotypic
388 diversity in response to environmental changes[17,29,30].
389 Previous research has highlighted the influence of plant tissue types on the
390 state of auxin response factor (ARF) biomolecular condensates[31]. The observation
391 of co-condensation between SUF4 and FRI in lateral roots, while absent in primary
392 roots of 6-13 days after germination plants, suggests the potential for a tissue-
393 specific functional relationship between these proteins. If this is true, we might
394 observe a tissue-specific change in mScarletI-FRI condensate behavior in response
395 to changes in SUF4 condensation. To test this hypothesis, we introduced FRI-
396 mScarletI into *suf4* null, 12S SUF4, and 5S SUF4 variant plants. At room
397 temperatures, we observed the formation of FRI-mScarletI condensates in about
398 10%-25% of primary roots of *suf4* null and 12S SUF4 plants, respectively (Fig.

399 6C, Table. 1; suf4 4/41, 12S SUF4 4/5), but no FRI-mScarletI condensates were
400 observed in the primary roots of rescue SUF4 (0/34) or 5S SUF4 lines (0/19). FRI-
401 mScarletI condensates were observed in a portion of lateral roots in all lines.
402 Although the number of mGFP-SUF4 condensates varies between rescue SUF4
403 and 5S SUF4, both genotypes have the ability to form condensates, whereas 12S
404 and *suf4* (*FRI*) do not. Thus, our data indicate an inverse relationship exists
405 between SUF4 and FRI condensates in the primary root. Furthermore, they suggest
406 that FRI is capable of forming at least two distinct types of condensates that vary
407 by tissue type: one type that assembles with SUF4, likely functioning to help
408 establish *FLC* transcription in newly formed tissue, and another type where the
409 proteins possibly act antagonistically.
410
411
412 **Table 1.** FRI-mScarletI condensate formation in different root types within SUF4
413 variants

	FRI Condensate formation			
	Lateral		**Primary**	
Genotype	Warm	Cold	Warm	Cold
FRI-mScarletI (*mEGFP-SUF4*)	Yes (n=8/29 roots)	?	No (n=0/34 roots)	Yes
FRI-mScarletI (*mEGFP-5S SUF4*)	Yes (n=2/6 roots)	?	No (n=0/19 roots)	Yes
FRI-mScarletI (*mEGFP-12S SUF4*)	Yes (n=2/2 roots)	?	Yes (n=4/5 roots)	Yes
FRI-mScarletI (*suf4 null*)	Yes (n=5/22 roots)	?	Yes (n=4/41 roots)	Yes

414
415 **SUF4 colocalizes with ELF7 in nuclear condensates at room temperature**
416 While FRI facilitates transcriptional activation of *FLC* by establishing a
417 permissive chromatin environment, other mechanisms have been shown to be
418 involved in the maintenance of *FLC* expression, such as transcriptional regulation
419 associated with histone H3 lysine 4 (H3K4) modifications [32,33]. In light of this, we
420 sought to investigate whether SUF4 condensates might serve as a hub for multiple
421 proteins involved in the transcriptional regulation of *FLC* by fluorescently tagging
422 and expressing EARLY FLOWERING 7 (ELF7), a known member of the PAF1
423 complex. We introduced mTFP-ELF7 expressed from its own upstream sequence
424 (pELF7::mTFP-ELF7) into rescue lines expressing mEGFP-SUF4 and mEGFP-
425 SUF4/FRI-mScarletI. ELF7 was specifically chosen due to its previous genetic

426 interaction with SUF4 and its role in establishing H3K4 activation marks on *FLC*,
427 as well as its physical co-localization with FRI in nuclear condensates under
428 normal temperature conditions[26,32,33]. Within both transgenic lines, we observed
429 mTFP-ELF7 to be diffuse within the nucleoplasm of cortical and epidermal cells
430 within the transition zone of both lateral and primary roots. In a subset of these
431 cells, mTFP-ELF7 formed 1-2 prominent nuclear condensates and occasionally
432 multiple smaller condensates (Fig. 5B).
433 As the introduction of mTFP-ELF7 did not appear to induce silencing, nor
434 alter condensate behavior in either the rescue mEGFP-SUF4 or mEGFP-
435 SUF4/FRI-mScarletI lines, we performed colocalization analysis using lines
436 expressing all three transgenes (Fig. 5B). While mEGFP-SUF4 formed more
437 condensates compared to ELF7 and FRI in nuclei analyzed (nSUF4condensates=
438 414, nELF7condensates= 53, nFRIcondensates= 34), the presence of an ELF7
439 condensate almost always coincided with a SUF4 condensate (47 out of 53 cases).
440 Further, out of these 47 ELF7-SUF4-containing condensates, we observed the
441 additional presence of a FRI condensate in 8 cases (17%). The quantitative
442 correlation between SUF4 condensation and flowering time, coupled with its
443 ability to co-localize with both FRI and ELF7 in 1-2 condensates, supports the
444 notion that SUF4 condensation likely functions in regulating the transcriptional
445 activity of *FLC* under different temperature conditions (Fig. 7).
446
447 **DISCUSSION:**
448 In this study, we have discovered that the IDP, SUF4, undergoes thermally-
449 regulated condensation both *in vitro* and *in planta*. These findings, along with the
450 demonstrated ability of SUF4 sequence alterations to progressively tune phase
451 separation, *FLC* transcription, and predictable flowering time outcomes, and the
452 evidence that SUF4 condenses with *FLC* transcriptional regulators under
453 appropriate physiological conditions, provide strong support for the hypothesis that
454 SUF4 phase separation may serve as a physical mechanism for plant temperature
455 perception. Our work emphasizes the biological importance of protein phase
456 separation in a multicellular organism by establishing links between
457 environmentally-sensitive phase separation, gene expression, development and
458 physiology.
459 Plant cells require an ability to filter out noise and interpret meaningful
460 signals from their environment to make developmental decisions. The
461 conformational promiscuity and multivalency of IDPs enables them to engage in a
462 variety of specific yet transient interactions under defined environmental
463 conditions. IDPs are enriched within plant proteomes, with many participating in
464 plant regulatory pathways and as integrators of environmental inputs[34–36]. The
465 phase separation states of such IDPs and client proteins could serve as an effective

466 mechanism for distinguishing real signals from noise within plant cells, thereby
467 enabling more efficient and effective developmental outcomes. Plants, along with
468 other organisms, use epigenetic factors, such as changes in chromatin/histone state,
469 signaling pathways, and RNA modifications to promote environmental-driven
470 developmental changes. However, these changes often require integration over a
471 significant period of time in order to induce a physiologically-relevant response.
472 Pairing IDP sensing with slower-acting epigenetic mechanisms may allow plants to
473 better distinguish genuine signals from noise by facilitating the promotion or
474 maintenance of molecular memory under persistent environmental cues. In the case
475 of SUF4, we found that changes in temperature cause it to phase transition between
476 condensed and uncondensed forms. Moreover, manipulating the
477 aromatic/hydrophobic properties of SUF4 proved to be sufficient to modulate its
478 material characteristics and tune the onset of flowering. Given SUF4's known
479 interaction with *FLC*-related chromatin remodelers and our cell biological
480 evidence that at least one of these co-condenses with SUF4 *in vivo*, these findings
481 suggest the possibility that SUF4 condensates could also associate with and alter
482 the activity of epigenetic factors to modulate *FLC* transcription.
483 Extensive investigations have shed light on the intricate regulation of
484 flowering time in *Arabidopsis*, with a specific emphasis on the transcriptional
485 modulation of *FLC*[1]. Among the key players in this regulatory network is FRI, an
486 interacting partner of SUF4[2,36]. Equipped with two coil-coil domains, FRI is
487 proposed to act as a scaffold protein, facilitating interactions with various *FLC*
488 transcriptional regulators and chromatin remodelers. Nevertheless, FRI itself does
489 not directly interact with the *FLC* gene locus. Instead, SUF4 serves as a mediator
490 of this interaction by physically binding both *FLC* and FRI, along with many other
491 members associated with the FRI complex [3,37]. Through both condensation and its
492 ability to recognize the *FLC* promoter region, SUF4 has the potential to enhance its
493 own activity by raising its local concentration, and also possibly by recruiting and
494 concentrating transcriptional activators (e.g. previously reported SUF4 interactors
495 FLX and TAF14), and chromatin remodelers (e.g. ELF7, SWC6, and RVB1) at the
496 *FLC* promoter. Meanwhile, we hypothesize that FRI transiently interacts with
497 SUF4, contributing to the establishment of transcriptional regulation of *FLC* in
498 newly formed tissues such as lateral roots. Newly developed and emerging
499 molecular images and technologies, such as those that enable the visualization and
500 quantitation of molecular events at a single genetic locus (e.g., endogenous
501 fluorescent tagging of gene loci via dCAS9/CRISPR), will aid in further
502 investigating the functional dynamics that govern these interactions at the *FLC*
503 gene locus.
504 The coacervation of prion-like proteins (PrLPs), such as FLL2 and FCA, has
505 recently emerged as a potential regulatory mechanism in flowering time [38].

However, it remains uncertain whether PrLP coacervation is thermally-driven, or even contributes to the post-transcriptional regulation of *FLC*. In this study, we demonstrate that a distinct proline-rich IDP undergoes LCST condensation behavior, which likely serves as a means to modulate flowering. This behavior aligns with the LCST observations of synthetic elastin-like polypeptides and Pab1 [22,39–42], which also possess a high proline content and repetitive hydrophobic features. While plants carry numerous proline-rich proteins and hybrid proline-rich proteins that are involved with abiotic- and biotic-associated pathways, the thermo-induced coacervation behavior of these proteins remains underexplored. By unraveling the role of proline-rich IDPs in phase separation and its relevance to flowering time regulation, our study extends our understanding of proline-rich IDPs in biological processes and sheds light on their potential participation in eukaryotic thermo-responses through phase separation phenomena. Moreover, our findings provide a strong basis for exploring the role of phase separation and environmental sensing, providing a valuable foundation and new insights into how we may be able to engineer plants and other organisms with tailored environmental responses.

Despite IDPs being often poorly conserved [43,44], SUF4 shares substantial homology with the animal protein BuGZ. In these organisms, BuGZ plays essential roles in both mitotic and transcriptional regulation by interacting with various cellular machineries, including the spindle assembly checkpoint protein (SAC) Bub3, the spliceosome, and epigenetic factors[10–12]. While SUF4's primary function in plants revolves around regulating flowering time, recent research has unveiled its potential involvement in analogous mitotic and transcriptional regulatory processes [45–47]. These newfound roles raise a series of questions, including whether SUF4's phase separation has evolved distinct functionality specific to plant flowering or if it serves as a universal mechanism within eukaryotic systems. Interestingly, animal BuGZ has been observed to undergo phase separation *in vitro*, and its role in phase separation is hypothesized to contribute to mitotic spindle formation. Therefore, studying SUF4 may not only advance our comprehension of how environmentally-induced phase separation impacts plant development and physiology but also hold significant promise in deepening our understanding of the broader evolutionary significance and functional implications associated with such environmentally-induced phase separation.

586 **MATERIALS AND METHODS:**
587
588 **Plant Material, accessions, and growth conditions**
589
590 All plants used in this study were grown under controlled conditions in
591 growth rooms with a light intensity of approximately 180 µmol m−2 s−1 at a
592 temperature of 21°C. Plants were either exposed to long day conditions (16 hours
593 of light followed by 8 hours of darkness).
594
595 *Col (FRI-SF2)* [48] was used as the wild-type accession for all genotypes analyzed in
596 this study. These lines are characterized as winter annuals and exhibit a delayed
597 flowering phenotype.
598
599 *suf4 (FRI-SF2)* plants [32] were used as the mutant accession for this study. These
600 plants carry an ~6kb deletion that spans the N-terminus of SUF4 (deleted region:
601 exons 1,2,3 and part of intron 3), resulting in a null mutation that causes an early
602 flowering phenotype.
603

Transgenic lines generated in this study
pSUF4::mEGFP-SUF4 in *suf4 (FRI-SF2)*
pSUF4::mEGFP-5SSUF4 in *suf4 (FRI-SF2)*
pSUF4::mEGFP-12SUF4 in *suf4 (FRI-SF2)*
pFRI::FRI-mScarletI; pSUF4::mEGFP-SUF4 in *suf4 (FRI-SF2)*
pFRI::FRI-mScarletI; pSUF4::mEGFP-5SSUF4 in *suf4 (FRI-SF2)*
pFRI::FRI-mScarletI; pSUF4::mEGFP-12SSUF4 in *suf4 (FRI-SF2)*
pFRI::FRI-mScarletI; pSUF4::mEGFP-30ISUF4 in *suf4 (FRI-SF2)*
pELF7::mTFP-ELF7; pSUF4::mEGFP-SUF4 in *suf4 (FRI-SF2)*
pELF7::mTFP-ELF7; pFRI::FRI-mScarletI; pSUF4::mEGFP-SUF4 in *suf4 (FRI-SF2)*
U2B"-mRFP(pROK2); pSUF4::mEGFP-SUF4 in *suf4 (FRI-SF2)*

604
605

606 **Flowering time quantification**
607 To assess flowering time in SUF4 variants, seeds of each genotype were
608 individually sown in Pro Mix BX soil and stratified at 4°C for two days. Then,
609 planted pots were transferred to either short day or long day chambers. The total
610 number of true rosette leaves was recorded every 3-5 days until plants bolted. To
611 minimize position effects, all genotypes were spatially mixed within their
612 respective short- or long day growth chambers.
613
614 **Cloning schemes:**
615
616 **pHM11 (rescue SUF4):**
617 To create pHM11 (pSUF4::6HIS-mEGFP-SUF4), a 2,981 fragment containing the
618 genomic SUF4 sequence was amplified using oHM3 (TTA GGA TCC GGT GGA
619 GGC GGT TCA GGC GGA GGT GGC TCT GGC GGT GGC GGA TCG ATG
620 GGT AAG AAG AAG AAG AGA), a forward primer with an added BamHI site
621 and a 3XGGGS linker, and oHM4 (GGC CTC GAG CTA AAA CGC CAT CCG
622 CCC AGC AA), a reverse primer with a 3' XhoI site. This fragment was then
623 cloned into pGEM-T easy to generate pHM1 (genSUF4). Additionally, the mEGFP
624 gene was amplified from addgene's commercially available mEGFP plasmid
625 (#18696) using oHM1 (ATA AGA TCT AGT GAG CAA GGG CGA GGA G), a
626 primer with a BglII 5' site, and oHM2 (ATG GAT CCC TTG TAC AGC TCG
627 TCC ATG CC), a primer with a 3' BamHI site. The resulting fragment was cloned
628 into pGEM-T easy to create pHM2 (mEGFP). Subsequently, pHM2 was digested
629 with BglII and BamHI, and then inserted into the pET-30a(+) vector, resulting in
630 pHM3 (6HIS-mEGFP). Plasmids pHM1 and pHM3 were then cleaved with BamHI
631 and XhoI and ligated, yielding pHM4 (6HIS-mEGFP-SUF4). A 1059 bp fragment
632 upstream of the SUF4 coding region was PCR amplified using oHM28 (ATC TTT
633 AAC TTT TTT GTT GTT GCA) and oHM24 (GAT GGC GCG CCC ACT AAA
634 TCT TTC TCC TA), a primer with an ASCI site, and inserted into the pGEM-T
635 easy vector, generating pHM5 (proSUF4). Additionally, a 332 bp region
636 downstream of the SUF4 coding region was PCR amplified using oHM25 (GAT
637 GGC GCG CCC TCG AGA ATT TGG CAC CAA ACC AA), a primer with both
638 ASCI XHOI restriction sites, and oHM17 (gaacaacatggtgcaaacatt), and cloned into
639 pGEM-T easy to produce pHM6 (termSUF4). Subsequently, pHM5 was digested
640 with SacII and AscI, and the resulting fragment was cloned into pHM6 to create
641 pHM7 (proSUF4::AscI-XhoI-3'UTR). pHM4 (6HIS-mEGFP-SUF4) was reverse
642 amplified to add a kozak consensus sequence using primers ohm45
643 (TTCACCAAAATGCACCATCATCATCATCAt) and oHM46
644 (GGcgcgCCCACTAAATCTTTCTCC), and then digested with AscI and XhoI for
645 cloning into pHM7, resulting in pHM10 (proSUF4::6HIS-mEGFP-SUF4-3'UTR).

646 For downstream biochemical assays requiring removal of mEGFP, an enterokinase
647 sequence was introduced before the SUF4 coding region using primers oHM35
648 (CGATCCGCCACCGCCAGAGCC) and oHM36
649 (gacgacgacgacaagATGGGTAAGAAGAAGAAGAGA), generating
650 pHM10_entero (proSUF4::6HIS-mEGFP-entero-SUF4-3'UTR). Subsequently,
651 pHM10_entero was cloned into pBIN30 via the NotI restriction site to make
652 pHM11 (proSUF4::6HIS-mEGFP-entero-SUF4-3'UTR).
653
654 **pHM32 (30I SUF4):**
655 To create pHM32, the last 1969 bp of SUF4's disordered region was synthesized
656 (GenScript, USA) with base pair substitutions that replaced all 30 alanine residues
657 with isoleucine residues. Gibson assembly was used to fuse this fragment with the
658 remaining 1012 bp genomic sequence of SUF4 to reassemble the complete gene.
659 Once the 30I SUF4 fragment was assembled, pHM10_entero and the 30I fragment
660 were cut with BamHI and XhoI and ligated together to make pHM31
661 (pSUF4::mEGFP-30ISUF4). Then, pHM31 was cut with Not1 and cloned into the
662 binary vector pBIN30 (Basta resistant) to make pHM32 (pSUF4::mEGFP-
663 30ISUF4).
664
665 **pHM14 (12S SUF4):**
666 To create pHM14, the last 1969 bp of SUF4's disordered region was synthesized
667 (GenScript, USA) with base pair substitutions that replaced 12 of the 14
668 phenylalanine and lysine residues with serines. Gibson assembly was used to fuse
669 this fragment with the remaining 1012 bp genomic sequence of SUF4 to
670 reassemble the complete gene. Once the 12S SUF4 fragment was assembled,
671 pHm10_entero and the 12S fragment were cut with BamHI and XhoI and ligated
672 together to make pHM12 (pSUF4::mEGFP-12SSUF4). Then, pHM12 was cut with
673 Not1 and cloned into the binary vector pBIN30 (Basta resistant) to make pHM14
674 (pSUF4::mEGFP-12SSUF4).
675
676 **pHM5S (5S SUF4):**
677 To create pHM5S, the last 1969 bp of SUF4's disordered region was synthesized
678 (GenScript, USA) with base pair substitutions that replaced the last 5
679 phenylalanine and lysine residues with serines. Gibson assembly was used to fuse
680 the remaining 1012 bp genomic sequence of SUF4 to reassemble the complete
681 gene. Once the 5S SUF4 fragment was assembled, pHm10_entero and the 5S
682 fragment were cut with BamHI and XhoI, and ligated together to make pHM13
683 (pSUF4::mEGFP-5SSUF4). Then, pHM13 was cut with Not1 and cloned into the
684 binary vector pBIN30 (Basta resistant) to make the final vector pHM5S
685 (pSUF4::mEGFP-5SSUF4).

686
687 **pFRI::FRI-mScarletI:**
688 pFRI::FRI-mScarletI was custom-synthesized by GenScript and consists of the
689 following elements: The FRI 1243 bp upstream promoter region with an added
690 Kozak consensus sequence (CACCAAA), directly followed by the 1351 bp FRI
691 (SF2) genomic region, 3XGGGS linker (GGT GGA GGC GGT TCA GGC GGA
692 GGT GGC TCT GGC GGT GGC GGA TCG), mScarletI sequence derived from
693 Addgene 98839, and FRI's putative 169 bp 3'UTR. Both promoter and 3'UTR
694 sequences were obtained from TAIR Sequence Viewer, whereas the genomic
695 sequence was provided by Sang Yeol Kim. The aggregated synthesized DNA was
696 flanked with NotI cut sites and subsequently inserted into the pBIN40 (Hyg
697 resistant) binary vector through NotI digestion and ligation.
698
699 **pELF7::mTFP-ELF7:**
700 pELF7::mTFP-ELF7 was custom synthesized by GenScript, USA and comprises
701 the following components: The ELF7 405 bp upstream promoter region with an
702 added Kozak consensus sequence (CACCAAA), directly followed by the mTFP
703 sequence (Addgene 55503), 3XGGGS linker (GGT GGA GGC GGT TCA GGC
704 GGA GGT GGC TCT GGC GGT GGC GGA TCG), the 3228 bp ELF7 genomic
705 region (TAIR), and the ELF7 putative 1791 bp 3' UTR. All promoter, genomic,
706 and 3'UTR sequences were obtained from TAIR Sequence Viewer. The
707 synthesized DNA was flanked by NotI sites, which were used for subsequent
708 insertion into the pBIN40 (Hyg resistant) binary vector.
709
710 **U2B"-mRFP (pROK2):** U2B" -mRFP (pROK2) was previously created by Alie
711 Pendle and Peter Shaw and commercially available for order via ABRC
712 (https://abrc.osu.edu/stocks/number/CD3-795056).
713
714 **Live Cell Microscopy and Fluorescence Recovery After Photobleaching**
715 **(FRAP)**
716
717 Live-cell imaging was performed on roots of 6-7 day old seedlings using either
718 point scanning or a spinning disk scanning confocal microscopy. Point-scanning
719 was performed on a Leica SP8 microscope equipped with HyD detectors, a white
720 light supercontinuum laser, and AOBS (Acousto-Optical Beam Splitter) control of
721 shuttering, excitation and emission bands. All images were acquired with a Leica
722 60x 1.3 N.A Plan-Apo glycerin immersion objective. Leica Lightning
723 deconvolution was used to improve signal to background for all point-scanning
724 images. Spinning disk confocal microscopy was performed either with a CSU-
725 W110 confocal head (Yokogawa) combined with a MESA Field-flattening device

726 (Intelligent Imaging Innovations) mounted on an Olympus IX83 microscope
727 equipped with a 100x Plan-Apo 1.35 NA silicon oil immersion objective, or a fully
728 automated Leica DMI6000B microscope equipped with a CSU-X spinning disk
729 confocal head (Yokogawa Corp.). Each sample was excited using 488nm for GFP
730 (Coherent cube laser), 561nm for mScarletI (Coherent cube laser), or 442nm for
731 mTFP (Coherent cube laser). Emitted light was collected with a 525/50 nm filter
732 for GFP, 605/64 nm filter for mScarletI and a 482/35 nm filter for mTFP (all filters
733 from Semrock).
734
735 FRAP experiments were conducted using the CSU-X spinning disk microscope
736 described above, with aid of a Vector laser scanning unit (Intelligent Imaging
737 Innovations) attached to the right camera port to focus and steer laser energy on the
738 image plane. The camera port was switched from imaging to bleaching paths via
739 software control (SlideBook, Intelligent Imaging Innovations) to alternate between
740 imaging and FRAP light paths. mEGFP-SUF4 was excited using 3.5 mW of light
741 energy (as measured at the end of the laser fiber entering the confocal head) from a
742 solid state 488nm laser (Coherent Technologies). Emission light was collected
743 using a 488nm dichroic mirror and 500-550nm emission filter (Semrock). Single-
744 plane Images were collected every 200ms using a Leica 100x Plan-Apochromat
745 100x 1.40 NA oil immersion objective and FRAP was performed within a 1.094
746 micron^2 region of interest centered on each assessed condensate spot using 5mW of
747 light energy as measured at the end of the fiber entering the Vector unit. The focal
748 spot was moved by galvometers to bleach a grid of spots separated by 20 nm
749 within the FRAP region. Seven frames were collected before bleaching and 143
750 frames were collected after bleaching (1.75 seconds to conduct bleaching, 0.2
751 second delay to first post-bleach acquisition). Once all images were acquired, they
752 were aligned in ImageJ [49] using the MultiStackReg plugin [50]. The Trackmate
753 plugin [51] was used to segment mEGFP-SUF4 spots for measurement of both the
754 mean fluorescent intensity and mobility of condensates over time (DoG detector,
755 estimated object diameter 0.6µm, sub-pixel localization, simple LAP tracker:
756 Linking max distance 1µm, Gap-closing distance 1µm, and Gap-closing max frame
757 gap 1). Afterwards, easyFRAP [52] (https://easyfrap.vmnet.upatras.gr/) was used to
758 calculate double normalized (initial intensity, photobleaching) FRAP values among
759 the different variants, with each curve undergoing a double exponential curve fit
760 (Normalization method: Double, Exponential Equation: Double, Data collected: T-
761 Half, Mobile Fraction, R-Squared).
762
763 **Live-cell imaging during temperature change**
764 Temperature change experiments were performed on the Leica SP8 microscope.
765 Seedlings were placed in a 4C growth chamber for 24 hours. Then, they were

766 mounted in ice water and moved onto the microscope stage, where they underwent
767 continuous imaging for 10 minutes. As a control, room temperature seedlings were
768 mounted in room temperature water and continuously imaged using the same
769 amount of time.
770
771 **Colocalization analysis**
772 Co-localization of mEGFP-SUF4 condensates with FRI-mScarletI, U2B", and/or
773 mTFP-ELF7 was investigated by collecting multichannel 3D datasets on the
774 spinning disk microscope with the CSU-W1 confocal head described above.
775 Images were acquired with a 100x Plan-Apo 1.35 NA silicon oil immersion
776 objective at 0.3µm intervals on the z-axis. The Spots function and Matlab plugin
777 for colocalization analysis in Imaris software (RRID:SCR_007370,
778 URL:http://www.bitplane.com/imaris/imaris) were used to segment condensate
779 signal and assess co-localization. Spot diameters of 0.5µm were used to detect and
780 determine the locations of mEGFP-SUF4, whereas FRI and U2B" condensates
781 were detected with a spot diameter of 0.7µm. These diameters values were
782 determined by assessing the diameter that worked best for segmentation of
783 condensate signal using the Imaris Spots function and were largely indicative of
784 the typical condensate diameters. Spots were considered co-localized if the
785 centroids of the spots (determined at a sub-pixel scale), were closer than the radius
786 of the smaller Spot size used to detect and segment mEGFP-SUF4 signal (0.25
787 µm).
788
789 **Puncta quantification**
790 To quantify SUF4 nuclear condensates, we auto-cropped individual nuclei from 3D
791 stacks using the NucleusJ2.0 auto crop function in Fiji. Subsequently, the cropped
792 images were imported into LabView, where a custom signal algorithm was applied
793 to normalize the signal loss due to light scattering and spherical aberration from the
794 top to the bottom of the z-stacks. To create the dataset used for normalization, we
795 isolated the diffuse EGFP-SUF4 signal within the nucleoplasm away from the
796 brighter SUF4 puncta via a set of binary masks, one mask for total SUF4 signal
797 above background and second mask for the puncta. The threshold for the total
798 mask was set by eye, and that for the puncta was created to include only pixels
799 falling between 0.02% and 20% below the maximum pixel value in the section. For
800 each section, the puncta signal was then subtracted from the total signal to obtain
801 the nucleoplasm signal, and the mean nucleoplasm value per pixel calculated. The
802 nucleoplasm signal was roughly linear to the focal depth once the focal plane was
803 within the nuclear volume, enabling us to model signal loss with a linear fit to the
804 mean intensity in these focal sections. The pixels in planes conjugate the nuclear
805 volume were normalized to the inverse of the fit line. The code for TIFF file

806 reading was shared online by Brian Hoover(forums.ni.com), the code for TIFF
807 multipage saving was shared online by Nico (forums.ni.com) and used with
808 modifications.
809
810 **Statistical analysis**
811 For the analysis of flowering time and condensate numbers, a nonparametric
812 Mann-Whitney U test was used to test for statistically significant differences
813 among sets of measurements made in different genotypes. For qPCR, FRAP and
814 motility results, a Student's two-tailed T-test for independent means was used. To
815 assess the significance of the observed co-localization frequency for FRI-mScarletI
816 and mEGFP-SUF4 condensates, we compared this frequency to that observed for a
817 control protein U2B"-mRFP, which forms 1-2 bodies per nucleus of similar sizes
818 to those observed for FRI-mScarletI. This experiment assumes that all three
819 proteins are localized to the nucleosol and allows for a statistical comparison
820 without knowing the spatial structure and volume of the nucleosol. A two-sample
821 (binomial) test of proportions was used to analyze the results.
822
823 **QPCR**
824 qPCR was employed to assess the transcript levels of both *SUF4* and *FLC*. To
825 achieve this, total RNA was extracted from six-day-old seedlings (approximately
826 20 seedlings per genotype) using the NucleoSpin RNA plant kit (Macherey-Nagel
827 CO.). Subsequently, 1 microgram of total RNA was reverse transcribed using the
828 QuantiTect Reverse Transcription kit (Qiagen). Real-time RT-PCR was performed
829 on 1:10 diluted cDNA using the SensiFAST SYBR No-ROX Kit (Bioline). Three
830 biological and technical replicates were analyzed per genotype, and ROC1
831 (AT4G38740) was used as a reference gene to normalize gene expression. The
832 reactions were carried out with an initial denaturation step at 95°C for 2 min,
833 followed by 45 cycles of 95°C for 5 s, 60°C for 10 s, and a final step at 72°C for 5
834 s.
835
836

Primer name	**Sequence**	**5' or 3'**	**Amplified gene**
FLC Forward	TCTCCTCCGGCGATAACCT	5'	*FLC*
FLC Reverse	GCATGCTGTTTCCCATATCGAT	3'	*FLC*

SUF4 Forward	AGGAATTCCACCCCATGTCTTGAC	5’	SUF4
SUF4 Reverse	CTGAGATTCGTCTGTCTATCGC	3’	SUF4
Cyclo Forward	CGATAAGACTCCCAGGACTGCCGA	5’	ROC1
Cyclo Reverse	TCGGCTTTCCAGATGATGATCCAACC	3’	ROC1

837
838
839 **Expression of His-mVenus-SUF4 in Sf9 cells**
840 Cloning and expression of His-mVenus-SUF4 was based on the Bac-to-Bac
841 Baculovirus Expression system (ThermoFisher). The control pFastBac-mVenus
842 and pFastBac-mVenus-SUF4 isoform 1 plasmids were obtained from Dr. Alex
843 Chin (*15*). In these vectors, mVenus was cloned solely or with an open reading
844 frame of SUF4 isoform 1 (NP_564369.1; 367 amino acid) in the modified
845 pFastBac vector (ThermoFisher). Site-directed mutagenesis was carried out to
846 create the 5S and 12S mutants using PrimeSTAR Max DNA polymerase (Takara-
847 bio). All plasmids were sequenced and verified prior to the transformation of
848 DH10Bac. Bacmid preparation, transfection and infection of Sf9 cells were
849 performed according to the manufacturer’s instruction. Large scale protein
850 expression was carried out by infecting and culturing the Sf9 cells with P3 viruses
851 for 2 days. Cells were centrifuged and either used immediately for protein
852 purification or frozen and stored at -80°C until use. Purification of His-mVenus-
853 SUF4 fusion protein from Sf9 cells. His-mVenus-SUF4 proteins were purified with
854 IMAC followed by gel filtration as published previously with some modifications.
855 All procedures were performed at 4°C. Proteins were extracted by sonicating the
856 cells in lysis buffer [50 mM Tris, 500 mM NaCl, 20 mM imidazole, 5 mM TCEP
857 (SIGMA, C4706), 5% glycerol, protease inhibitor cocktail (SIGMA, S8830) pH
858 7.44] supplemented with benzonase nuclease (SIGMA, E1014). The lysate was
859 cleared by centrifugation at 20,000 x g, for 20 min at 4°C, filtered with 0.45 µm
860 PVDF membrane filter (Millipore, SLHV033RS) and loaded onto Ni-NTA
861 columns (QIAGEN, 30230). After washing with the lysis buffer, proteins were
862 eluted with 500 mM imidazole (lysis buffer supplemented with 480 mM
863 imidazole). The eluate was concentrated using a centrifugal filter device, Amicon
864 Ultra-15 (Millipore, UFC901024) and loaded to a gel filtration column Superdex
865 200 Increase 10/300 GL operated with AKTA Pure 25L (GE Healthcare). Gel

866 filtration was performed in the Size Exclusion Chromatography (SEC) buffer (20
867 mM Hepes, 225 mM NaCl, 1 mM TCEP pH 7.4) with a constant flow rate of 0.4
868 ml/min. Typically, His-mVenus-SUF4 and His-mVenus proteins were eluted at
869 11.0 and 15.5-ml after the protein loading, respectively. Obtained fractions were
870 analyzed with SDS-PAGE, combined and concentrated. Protein concentration was
871 determined with Bradford protein assay kit (Thermo, 23200) using BSA as a
872 standard.
873
874 **Turbidity assay**
875 His-mVenus or His-mVenus-SUF4 proteins were thawed and ultracentrifuged to
876 remove denatured proteins. After protein concentration was determined, the protein
877 sample was diluted to 50, 25, 12.5, 6.25 and 3.13 μM in SEC buffer. Each sample
878 was mixed well with equal volume of turbidity assay buffer (20 mM Hepes, 75
879 mM NaCl, pH 7.4) to make a 250 μl reaction mix and transferred into a quartz
880 cuvette (Starna Cells, 28F-Q-10). Temperature-dependent phase transition was
881 detected by measuring the optical scattering at 800 nm while increasing the
882 temperature from 4 to 60°C (with a ramping rate of 0.5°C/min) using a
883 spectrophotometer Cary 300UV-VIS (Agilent Technologies). Nitrogen gas purging
884 was used to prevent the moisture from condensing on the cuvette surface. Three
885 replicates were performed for each sample.
886
887 **Droplet formation assay**
888 Five microliter of 50 μM proteins prepared as described above were mixed with 5
889 μl of turbidity assay buffer on ice and incubated for 5 min at 37°C. Each 3 μl of
890 protein reaction mix was loaded into a flow-chamber and immediately observed
891 with a confocal microscope SP5 (Leica) equipped with a 60x oil objective (NA
892 1.42). Imaging was performed with both DIC and fluorescence (excitation at 514
893 nm, emission 530 nm).
894
895
896
897
898
899
900
901
902

926

927 **FIGURES:**

928

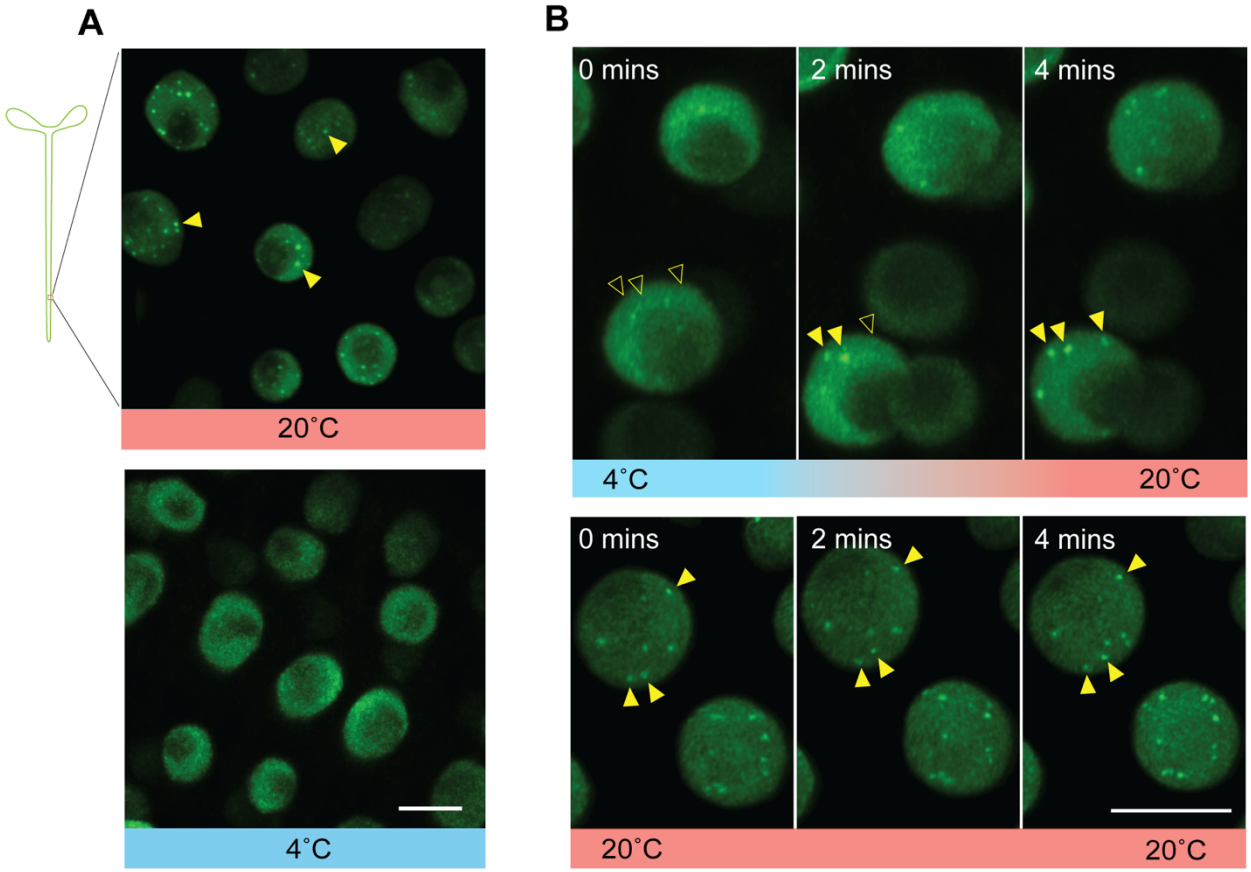

929

930

931 **Figure 1. SUF4 forms nuclear condensates that are sensitive to temperature *in***
932 ***planta*. A) mEGFP-SUF4 is expressed from native expression sequences in a**
933 **null mutant background, *suf4* (FRI).** mEGFP-SUF4 is diffuse within the
934 nucleoplasm and forms nuclear condensates at room temperature. However, at 4°C,
935 condensates do not form, leaving SUF4 diffused in the nucleoplasm. **B)** mEGFP-
936 SUF4 rapidly forms condensates as temperatures increase. Scale bar: 10µm, yellow
937 arrowheads point to the locations of nuclear condensates (filled) or locations where
938 they will appear in later images (empty).

939

940

941

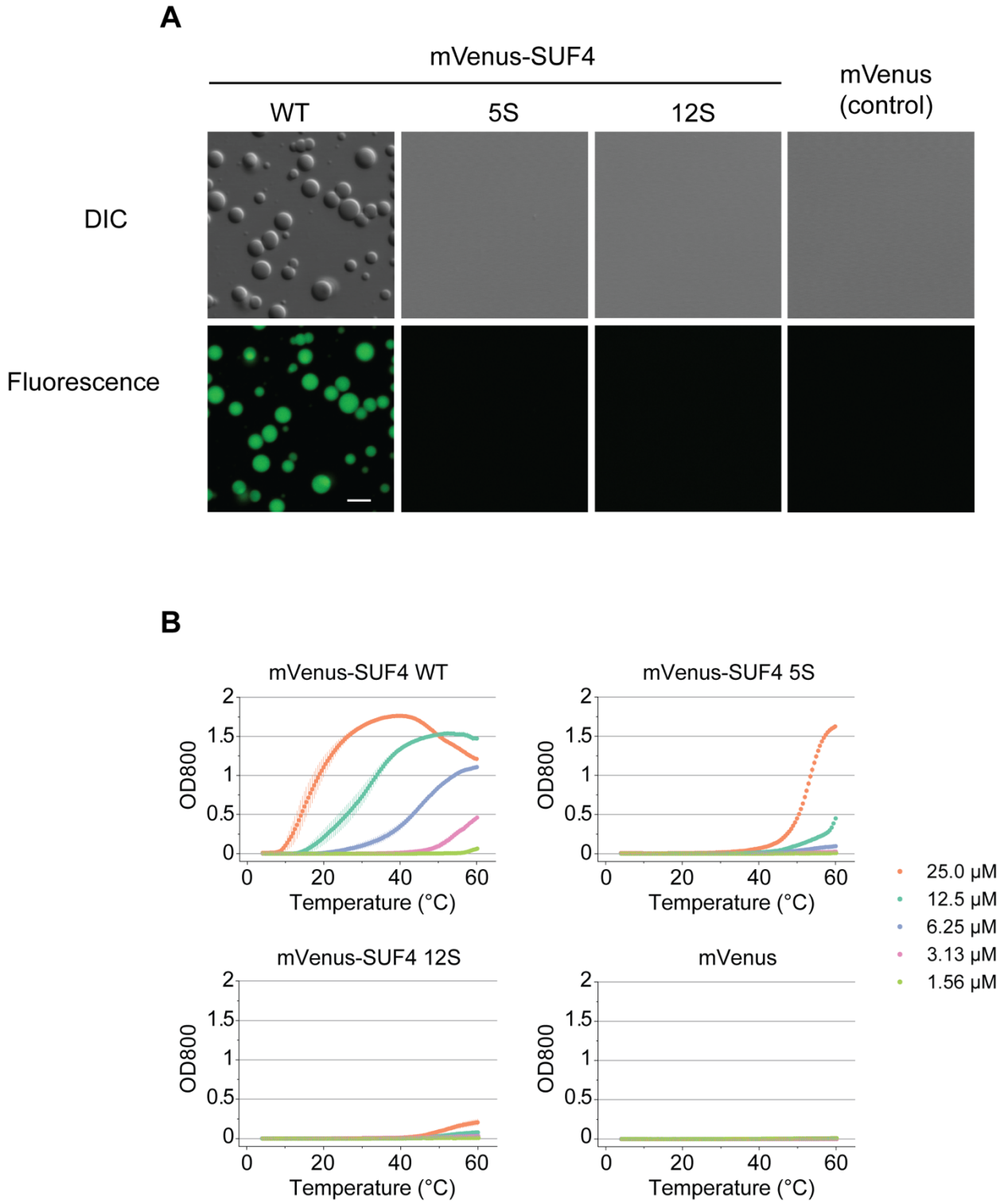
A
mVenus-SUF4
WT
5S
12S
mVenus
(control)
DIC
Fluorescence
B
mVenus-SUF4 WT
mVenus-SUF4 5S
mVenus-SUF4 12S
mVenus
OD800
Temperature (°C)
0
0.5
1
1.5
2
0
20
40
60
25.0 μM
12.5 μM
6.25 μM
3.13 μM
1.56 μM

942

943

944

945 **Figure 2. SUF4 forms temperature-sensitive condensates that may be tuned *in***
946 ***vitro*. A)** DIC and confocal images of purified SUF4 variants. Only rescue SUF4
947 forms condensates at 37°C. Scale bar:5µm. B**)** Turbidity assay demonstrating the
948 temperature sensitivity of purified SUF4 variants. The thermal set points shift
949 depending on the severity of amino acid substitutions and the concentration used.
950 Each graph includes three replicates for each sample, error bars depict standard
951 errors.

952
953
954
955
956
957
958

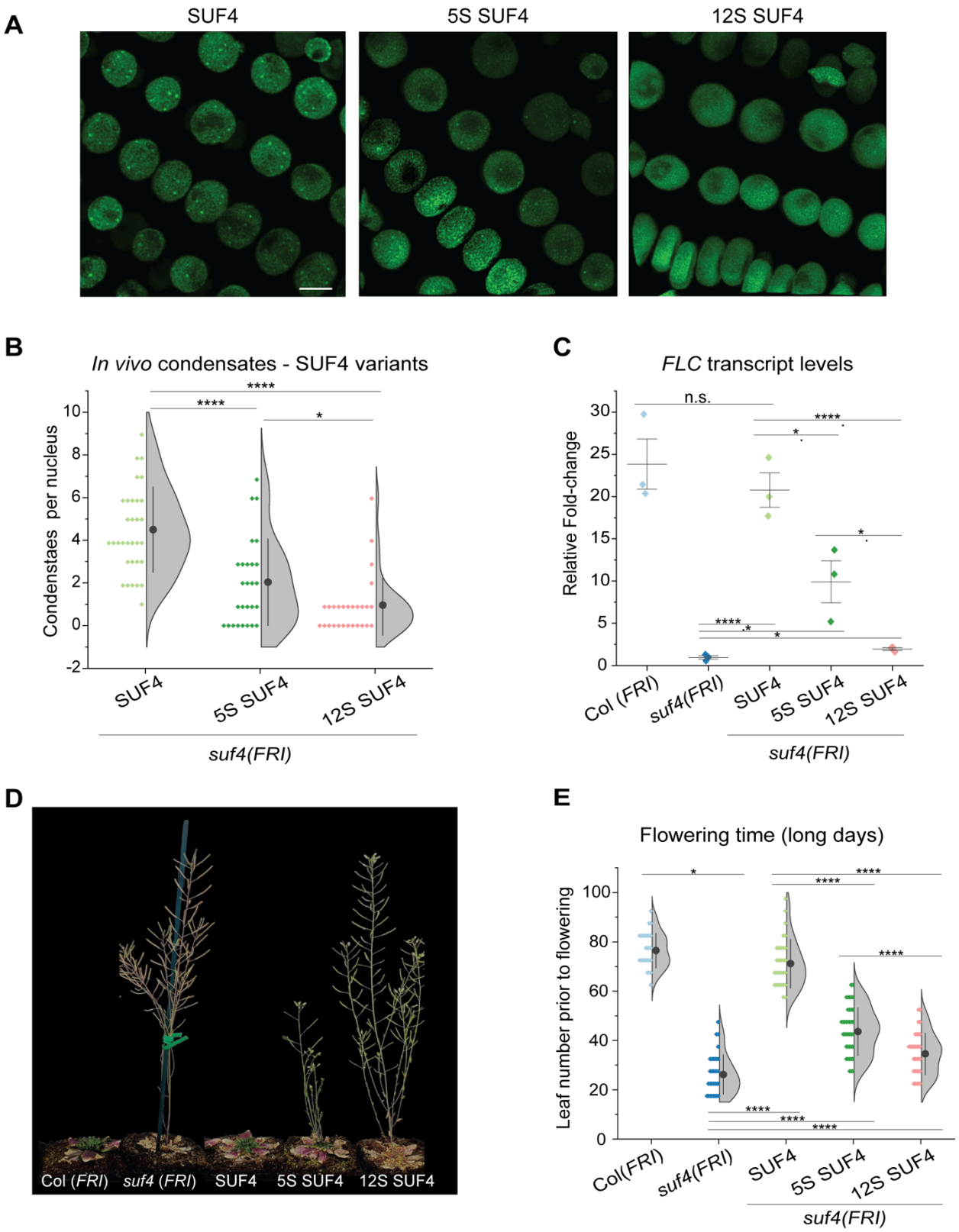
A
SUF4
5S SUF4
12S SUF4
B
In vivo condensates - SUF4 variants
Condenstaes per nucleus
SUF4
5S SUF4
12S SUF4
suf4(FRI)
C
FLC transcript levels
Relative Fold-change
n.s.
Col (FRI)
suf4(FRI)
SUF4
5S SUF4
12S SUF4
suf4(FRI)
D
Col (FRI)
suf4 (FRI)
SUF4
5S SUF4
12S SUF4
E
Flowering time (long days)
Leaf number prior to flowering
Col(FRI)
suf4(FRI)
SUF4
5S SUF4
12S SUF4
suf4(FRI)

962 **Figure 3. Tuning SUF4 condensate behavior corresponds to changes in**
963 **flowering time outcomes. A)** Confocal images of SUF4 variants, illustrating
964 varying condensation patterns. Rescue mEGFP-SUF4 forms an average of 4-5
965 nuclear condensates; 5S SUF4 forms 2-3 nuclear condensates on average; 12S
966 SUF4 shows 0-1 condensates on average. Scale bar: 5µm. **B)** Quantification of
967 panel A. Statistical analysis was performed by Mann-Whitney U test. **C)** Relative
968 abundance of *FLC* transcripts in different SUF4 variants. Rescue SUF4 shows *FLC*
969 transcript levels similar to WT, while various substitutions lead to graded
970 reductions. Statistical analysis conducted using a two-tailed Student's t-test for
971 independent means. Error bars represent the standard deviation. **D)** Image
972 comparing the flowering time phenotypes of plants expressing various mEGFP-
973 SUF4 variants with those of wildtype Col *(FRI)* plants. From left to right: Col
974 *(FRI)* showing delayed flowering, *suf4* (FRI) mutant displaying early flowering,
975 rescue mEGFP-SUF4 (functional copy of SUF4) expressed in *suf4 (FRI)* restoring
976 the delayed flowering phenotype, 5S SUF4 (5 Y and F substitutions for S)
977 expressed in *suf4 (FRI)* exhibiting a weak early flowering phenotype, and 12S
978 SUF4 (12 F and Y substitutions for S) expressed in *suf4 (FRI)* showing a moderate
979 early flowering phenotype. **E)** Quantification of panel D. Statistical analysis
980 performed by Mann-Whitney U test. Asterisks denote specific p-values * <0.01, **
981 <0.001, ***<0.001, and ****<0.0001. Error bars are standard deviation.

982
983
984
985
986
987
988
989
990
991

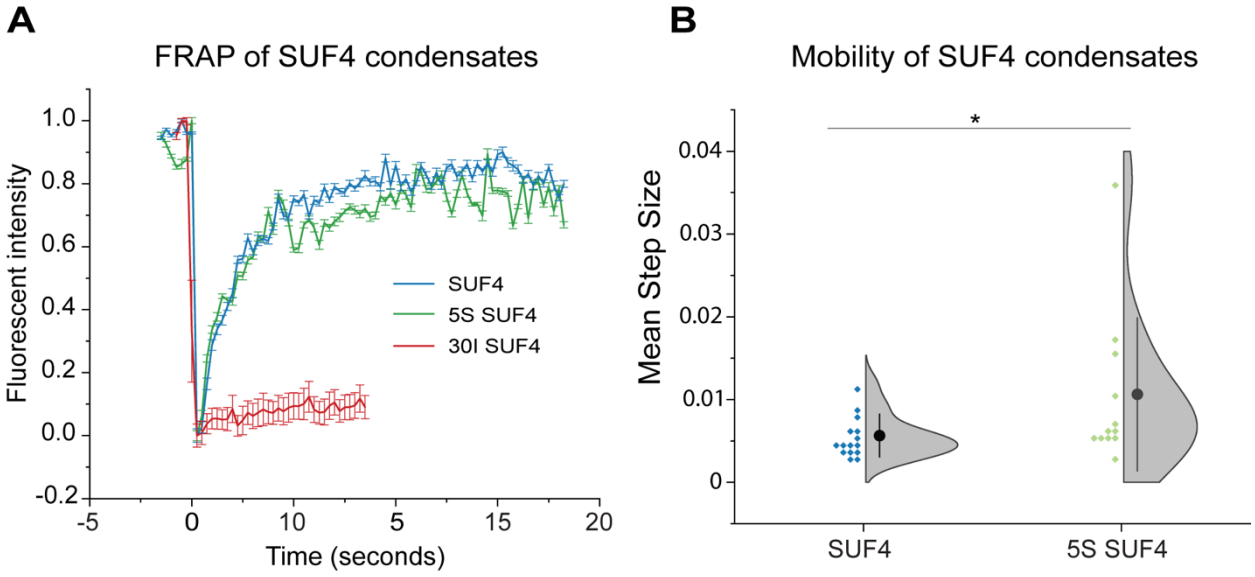

992
993

994

995 **Figure 4. SUF4 variants exhibit altered exchange rate and mobility dynamics**
996 **A)** Fluorescence Recovery After Photobleaching (FRAP) analysis of SUF4
997 variants reveals different recovery rates. 5S SUF4 exhibits the fastest recovery rate
998 (t1/2=0.85 seconds), followed by rescue SUF4 (t1/2=1.27 seconds). 30I SUF4 does
999 not recover within the duration of the experiment. **B)** Quantification of the total
1000 distance traveled for condensates used in panel A). On average 5S condensates
1001 were more mobile. Asterisks denote P-values from Student's T- test * <0.01
1002 FRAP distributions between rescue and 5S SUF4 were assessed for significance
1003 using a two-tailed Student's t-test (p-value=0.007). Error bars= standard deviation.

1004

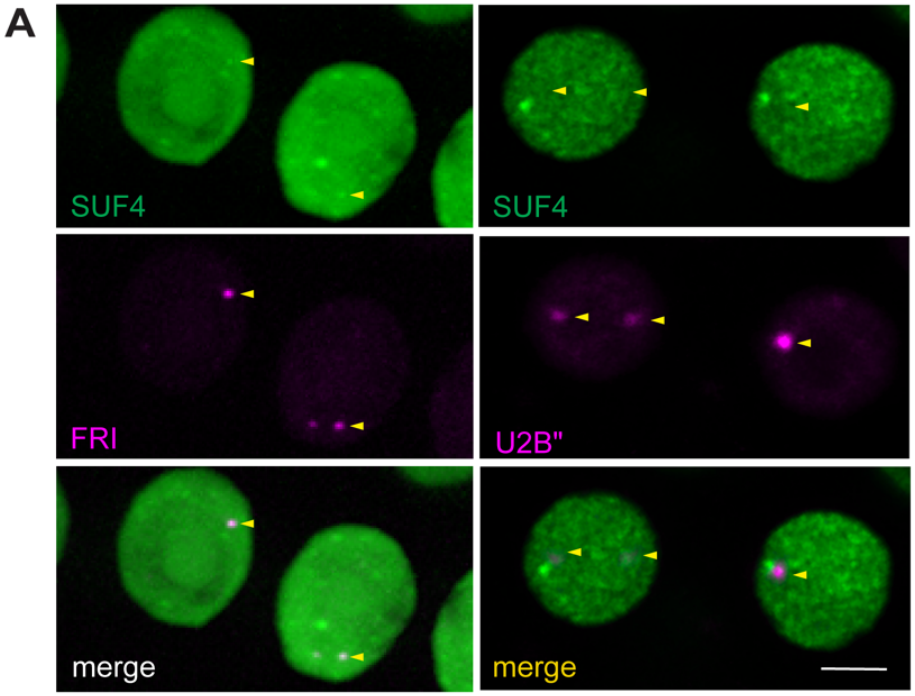

Spots 3D detection

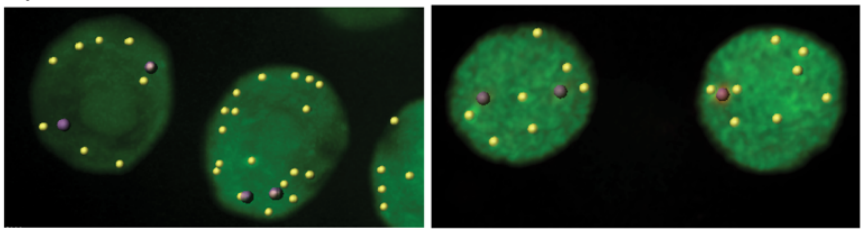

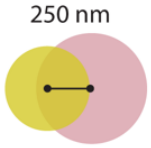

	FRI	U2B"
condensates	56	19
SUF4 colocalization	38	0
proportion	68%	0%
binomial test	$p<0.001$	

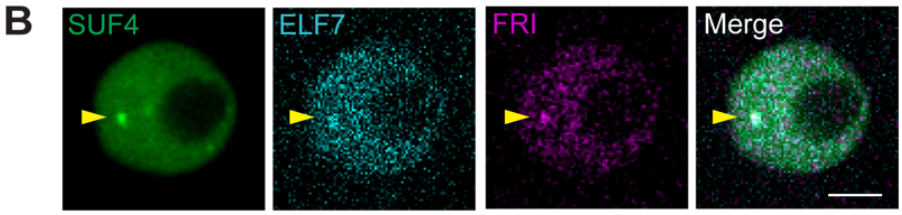

SUF4+FRI+ELF7: 17% of nuclei (n=47)

1006 **Figure 5. In warm temperature conditions, SUF4 co-localizes with members of**
1007 **the vernalization complex in newly derived meristematic tissues. A)** SUF4 and
1008 FRI co-localize in nuclear condensates within developing lateral roots at room
1009 temperatures. FRI is visualized by expression of mScarletI-FRI. mScarletI-FRI co-
1010 localization appears to be selective, as U2B", a protein found in nuclear splicing
1011 speckles, does not co-localize with SUF4. U2B" is visualized by expression of
1012 U2B"-mRFP. Binomial tests of proportions used to test for statistical significance.
1013 Arrowheads point to locations of tagged FRI or U2B" puncta. **B)** ELF7, a
1014 chromatin remodeler that functions with SUF4 and FRI to transcriptionally activate
1015 *FLC,* is visualized as mTFP-ELF7. mTFP-ELF7 also co-localizes within SUF4-
1016 FRI condensates. Arrowheads point to a nuclear body with signal concentration in
1017 all three channels. Scale bars: 5µm
1018

1019

1020

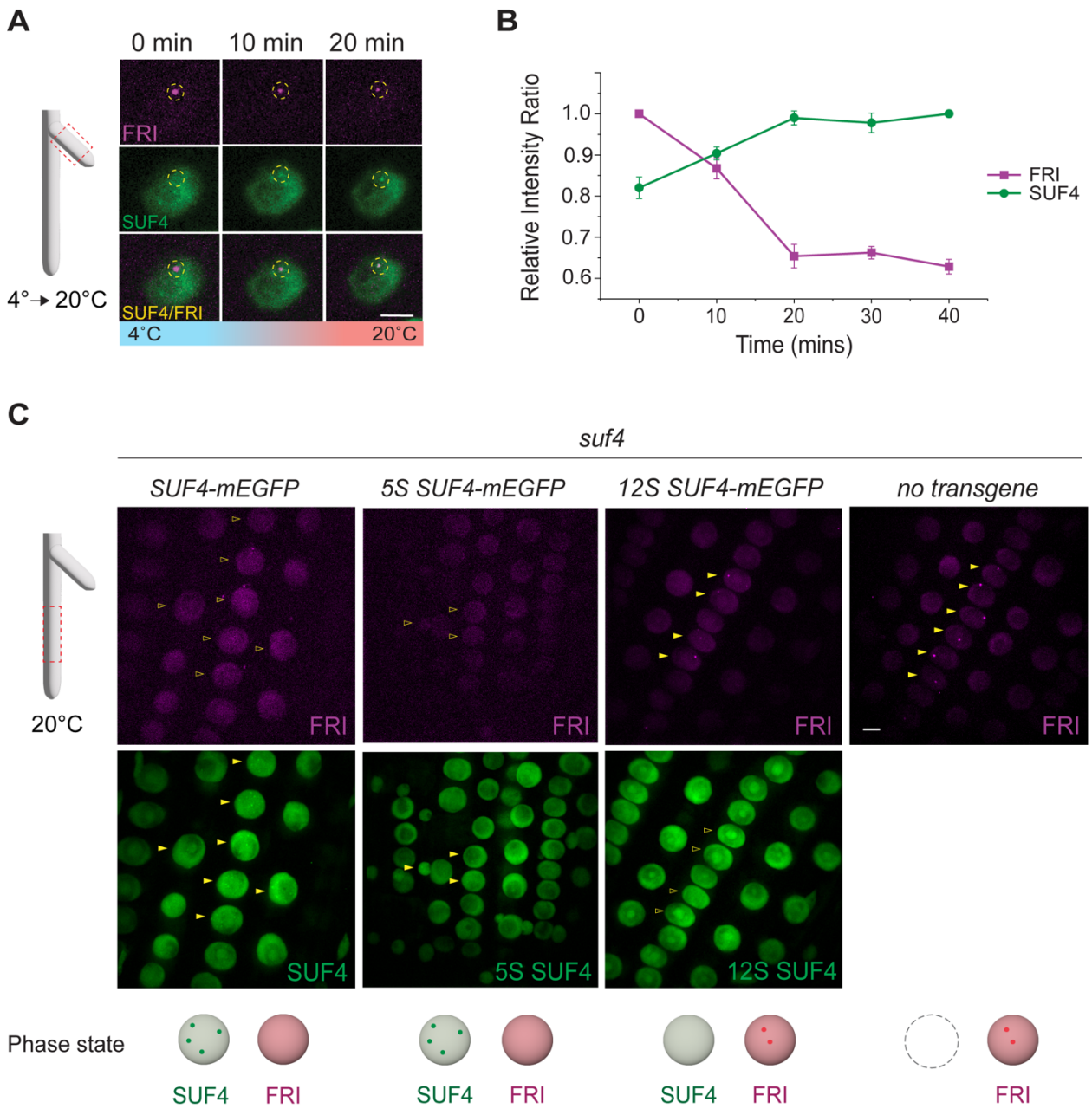

1021

1022

1023

1024

1025

1026

1027

1028 **Figure 6. SUF4 and FRI have different localization patterns under cold**
1029 **temperatures A and B**) Cold-induced FRI condensates do not co-localize with
1030 SUF4. However, these condensates can exchange positions with SUF4 nuclear
1031 condensates upon warming. **A)** The first 20 minutes of an imaging series,
1032 showcasing the phase change behavior of FRI and SUF4 as temperatures rise.
1033 Dotted circle is not the ROI used for quantification but used to mark diminishing
1034 and appearing condensates. **B)** Graph quantifying the opposing behavior of FRI
1035 and SUF4 condensation state at four locations from the same times series shown in
1036 A) (40 minutes, five time points). Error bars are standard errors. **C)** SUF4
1037 condensates spatially limit the formation of FRI condensates in the primary root. In
1038 SUF4 variant lines lacking condensates (12S and *suf4* mutants), FRI-mScarletI
1039 condensates begin to emerge. Schematic representing the phase state of SUF4
1040 (green circles) and FRI (magenta circles) in nuclei of each genotype. Scale bars in
1041 all panels: 5µm.

1042

1043

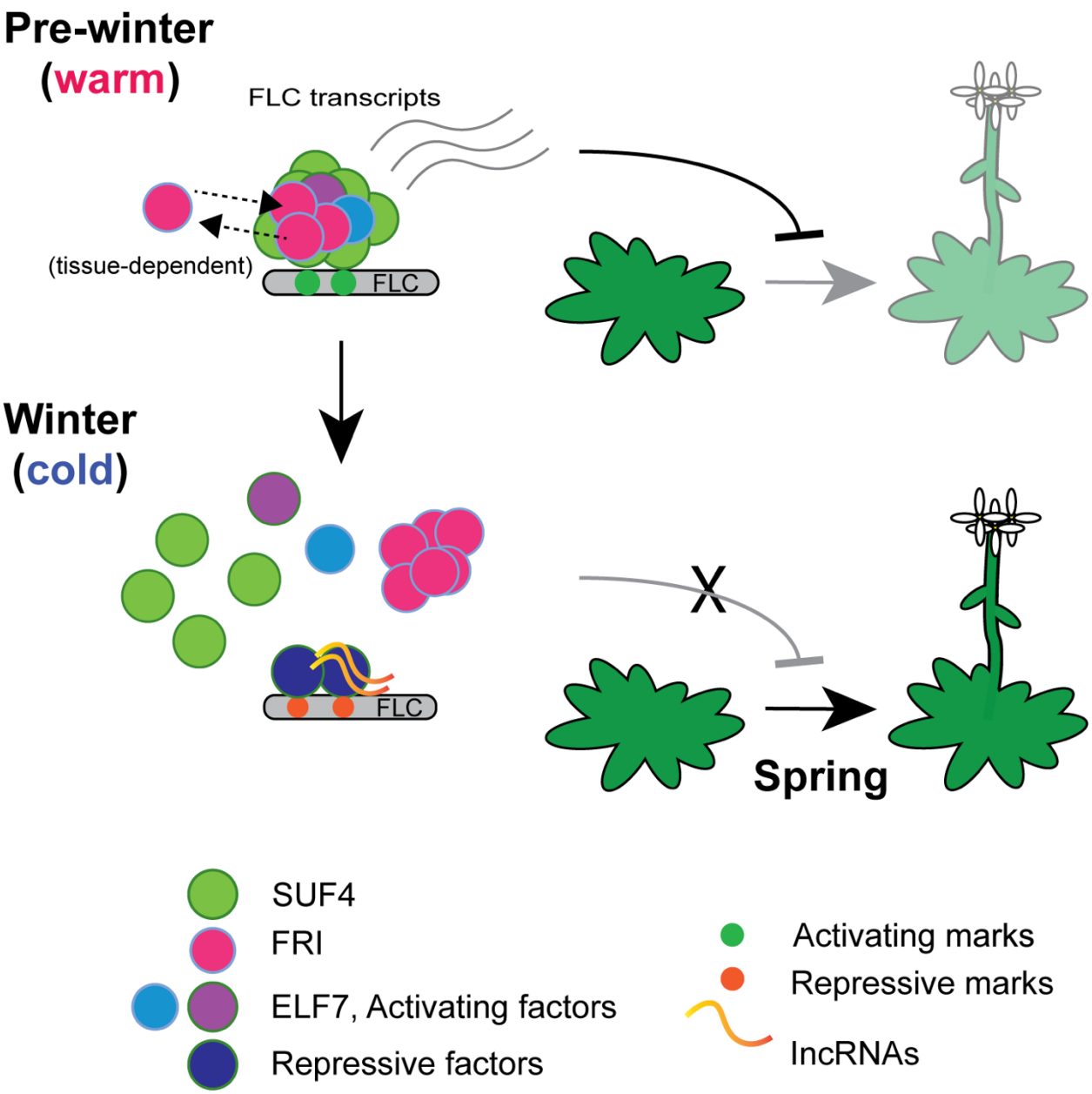

1044

1045

1046

1047

1048

1049

1050 **Figure 7: Proposed Model for Flowering-Time Regulation.** A proposed model
1051 for the regulation of flowering time mediated by SUF4 biomolecular condensates.
1052 SUF4 (green) biomolecular condensates function to concentrate and/or recruit
1053 members of the vernalization complex, including FRI (in red), ELF7 (in blue), and
1054 other associated factors (in purple) to the *FLC* gene locus. Certain members, such
1055 as FRI, exhibit transient localization within these condensates dependent on cell
1056 state. Condensate localization ultimately leads to the transcriptional activation of
1057 the *FLC* gene, resulting in the delay in flowering time. In response to cold
1058 temperatures, SUF4 condensates undergo disassembly. This disassembly may
1059 facilitate the recruitment of a new group of chromatin remodelers and the
1060 involvement of lncRNAs, both of which work together to transcriptionally silence
1061 the *FLC* gene. Transcriptional silencing of FLC is a necessary step for plants to
1062 undergo the floral transition and flower in the subsequent spring season.
1063
1064
1065
1066
1067
1068
1069
1070
1071
1072
1073
1074
1075
1076
1077
1078
1079

Supplementary Materials

A

suf4 (FRI) Col *(FRI)* *SUF4* / *suf4 (FRI)*

B

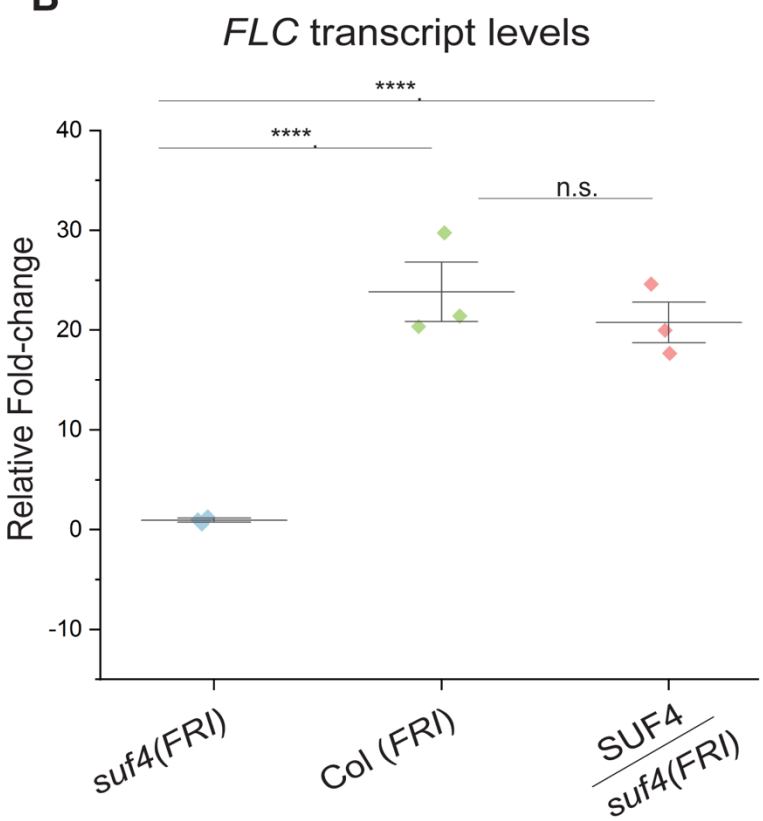

1081

1082
1083 **Supplemental Figure 1.** Expression of the pSUF4::mEGFP-SUF4 transgene
1084 rescues the *suf4* mutant phenotype **A)** Image of plants demonstrating the ability of
1085 the pSUF4::mEGFP-SUF4 transgene to rescue the *SUF4* flowering time
1086 phenotype. From left to right: *suf4 (FRI)* mutant plants displaying an early
1087 flowering time phenotype, Col *(FRI)* plants displaying a WT delayed flowering
1088 time phenotype, SUF4/*suf4 (FRI)* displaying a rescued WT delayed phenotype. **B)**
1089 Relative abundance of *FLC* transcripts in *suf4* mutant, Col *(FRI)*, and *SUF4 (FRI)*
1090 shown in A). Rescue SUF4 shows FLC transcript levels similar to WT. These data
1091 are reshown in Figure 2E. Statistical analysis conducted using a Student's t-test.
1092 Error bars represent the standard deviation. Asterisks denote the p-values* <0.01,
1093 ** <0.001, ***<0.001, and ****<0.0001.
1094
1095
1096
1097
1098
1099
1100
1101
1102
1103
1104
1105
1106
1107
1108
1109
1110

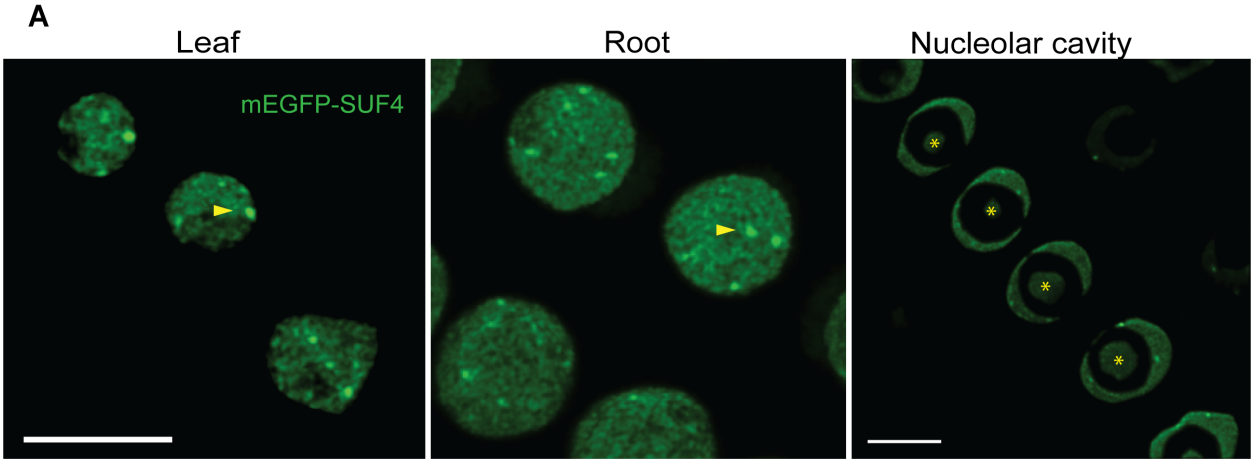

Supplemental Figure 2. At room temperatures, SUF4 forms biomolecular condensates in shoot cells, primary root cell, and localizes in the nucleolar cavity. Arrows point to nuclear condensates whereas stars mark the nucleolar cavity. Leaf and Root images are 3D rendered Z-stacks whereas the nucleolar cavity image is a slice from a 3D stack. Scalebar: 10 µm

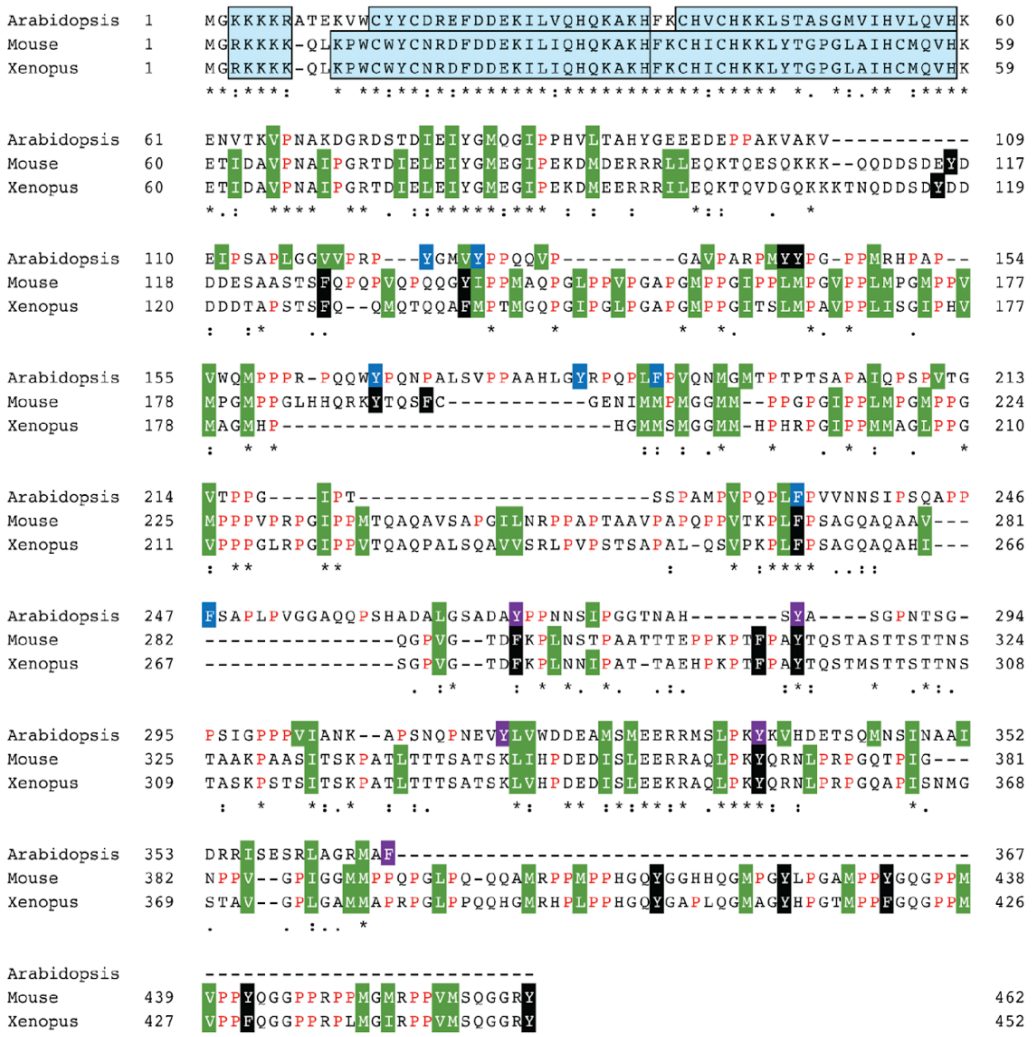

Supplemental Figure 3. Sequence alignment of *Arabidopsis* SUF4, mouse and Xenopus BuGZs. N-terminal domain that contains predicted NLS and zinc fingers (highlighted in cyan), is conserved well among three SUF4/BuGZ sequences whereas the central/C-terminal disordered domain of *Arabidopsis* SUF4 seems diverged from animal BuGZs. F and Y residues in the predicted disordered region are highlighted in black, blue, or purple. Other strong hydrophobic residues are highlighted in green. Among F and Y in the predicted disordered region of SUF4, the last 5 F and Y (highlighted in purple) were mutated to S in the 5S mutant and additional 7 F and Y at the central region (highlighted in blue) were mutated to the S in the 12S mutant.

1152

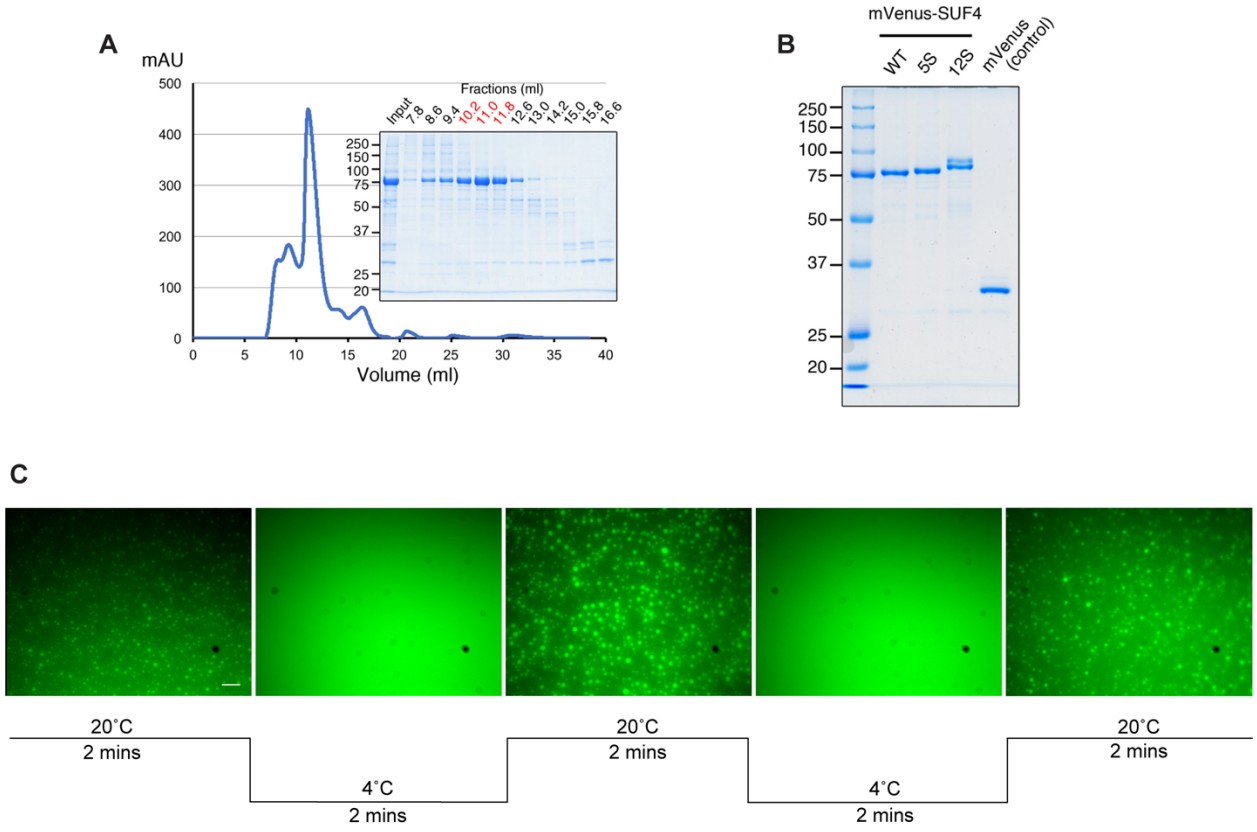

1153

1154

1155 **Supplemental Figure 4.** Purified SUF4 forms round and reversible liquid-like
1156 condensates *in vitro*. **A)** A representative elution profile of His-mVenus-SUF4 on
1157 gel filtration chromatography. Recombinant proteins were expressed in Sf9 insect
1158 cells, purified with IMAC, followed by gel filtration. Fractions were eluted around
1159 11-ml after sample loading to enrich for the fusion proteins (indicated with red
1160 letters in the inset of the gel image of fractions). **B)** SDS-PAGE analysis of the
1161 purified His-mVenus-SUF4 and control HIS-mVenus proteins. Note that 12S
1162 mutant protein has two bands on gel. **C)** Purified SUF4 forms round and reversible
1163 liquid-like condensates *in vitro*. SUF4 can undergo multiple rounds of temperature
1164 shifts without transitioning into a more stable gel or solid-like aggregate. Prior to
1165 temperature shifts, SUF4 is incubated at either 20˚C to 4˚C for 2 minutes. Upon
1166 temperature shifts every two minutes, SUF4 changes its phase state and maintains
1167 this behavior until the next shift. Scalebar: 45µm.

1168

1169

1170

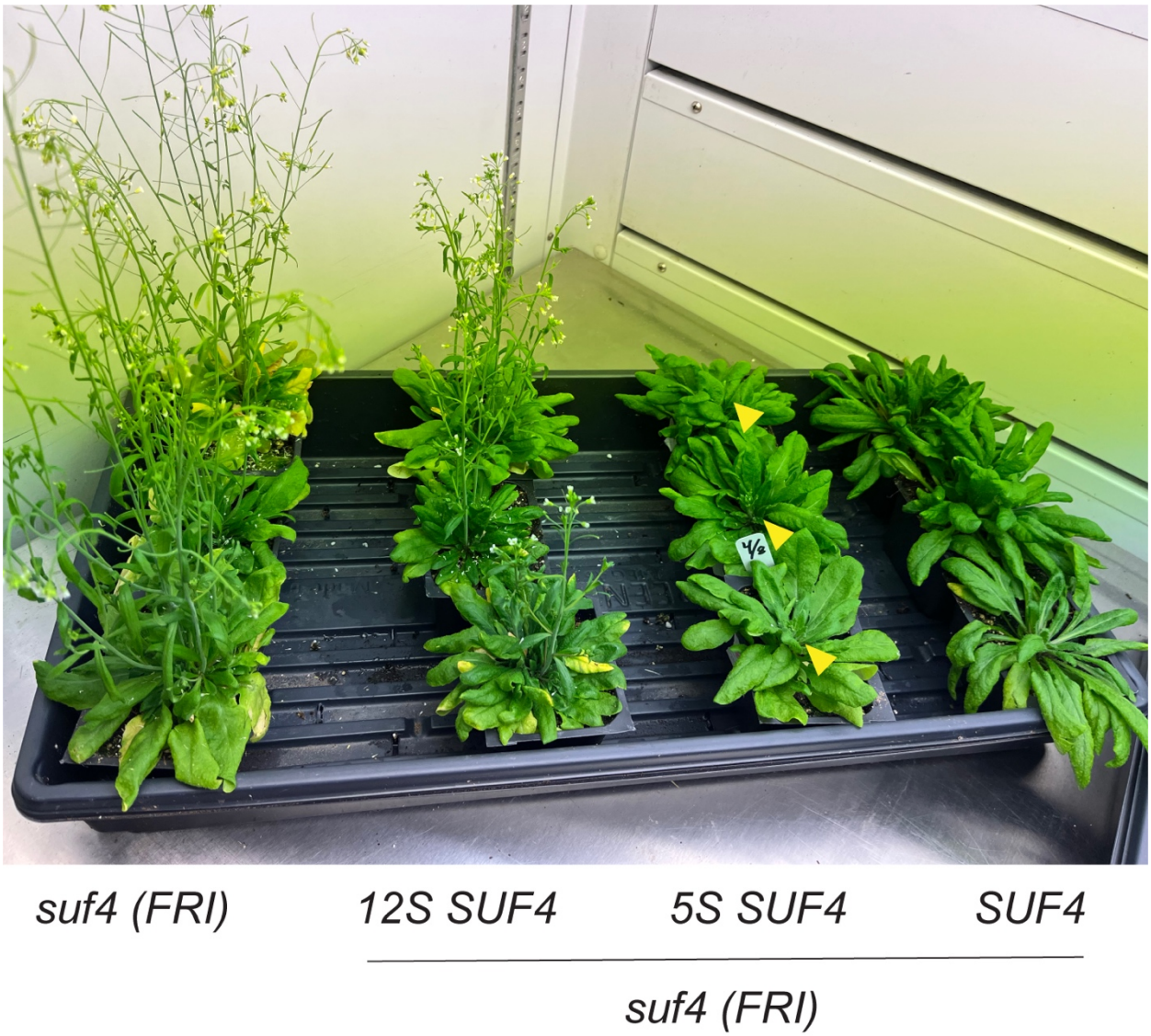

1171

1172 **Supplemental Figure 5. Image of SUF4 variants in comparison to mutant**
1173 ***suf4*, which flowers early.** Left to right: *suf4 (FRI)* mutant with an early flowering
1174 time phenotype, 12S SUF4 (12 F and Y substitutions for S) with a moderate early
1175 flowering phenotype, 5S SUF4 (5 Y and F substitutions for S) with weak early
1176 flowering phenotype, rescue mEGFP-SUF4 (functional copy of SUF4) rescuing
1177 the delayed flowering time phenotype.

1178

1179

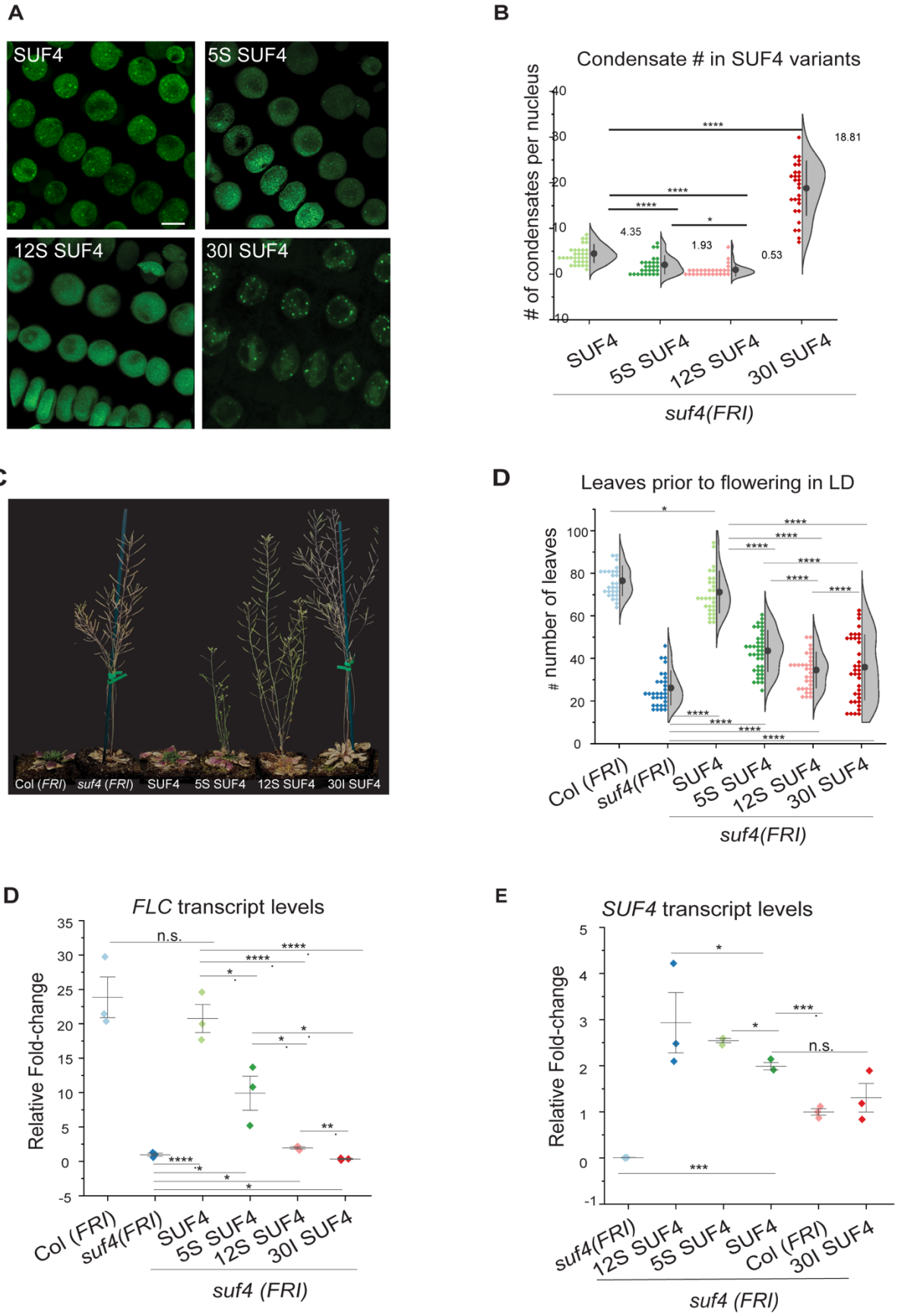
A
SUF4
5S SUF4
12S SUF4
30I SUF4
B
Condensate # in SUF4 variants
# of condensates per nucleus
4.35
1.93
0.53
18.81
SUF4
5S SUF4
12S SUF4
30I SUF4
suf4(FRI)
C
Col (FRI)
suf4 (FRI)
SUF4
5S SUF4
12S SUF4
30I SUF4
D
Leaves prior to flowering in LD
number of leaves
Col (FRI)
suf4(FRI)
SUF4
5S SUF4
12S SUF4
30I SUF4
suf4(FRI)
D
FLC transcript levels
Relative Fold-change
n.s.
Col (FRI)
suf4(FRI)
SUF4
5S SUF4
12S SUF4
30I SUF4
suf4 (FRI)
E
SUF4 transcript levels
Relative Fold-change
n.s.
suf4(FRI)
12S SUF4
5S SUF4
SUF4
Col (FRI)
30I SUF4
suf4 (FRI)

1180

1181 **Supplemental Figure 6.** Characterization of 30I SUF4 in relation to the remaining
1182 SUF4 variants. **A)** Confocal images showing that 30I SUF4 assembles into more
1183 nuclear condensates than SUF4 rescue. Scale bar: 5µm. **B)** quantification of A).
1184 30I SUF4 forms an average of ~18 condensates per nucleus). **C-D)** Leaf counting
1185 assay of different variants in long- and short-day conditions. Note that 30I SUF4
1186 does not rescue the flowering time phenotype. Statistical analysis done using a
1187 Mann-Whitney U test. **E)** Relative abundance of *FLC* transcripts in 30I compared
1188 to different SUF4 variants. 30I SUF4 does not rescue *FLC* transcript levels. **F)**
1189 qPCR of *SUF4* in 30I and other transgenic *SUF4* variant lines. 30I SUF4 exhibits
1190 similar levels of transcripts as the rescue SUF4 line. Statistical analysis for E) and
1191 F) conducted using a two-tailed Student's t-test for independent means. Error bars
1192 represent the standard deviation. All data other than 30I SUF4 are reproduced from
1193 the main figures. Asterisks denote P-values * <0.01, ** <0.001, ***<0.001, and
1194 ****<0.0001

1195
1196
1197
1198
1199
1200
1201
1202
1203
1204
1205

1206

1207
1208

1209
1210

1211

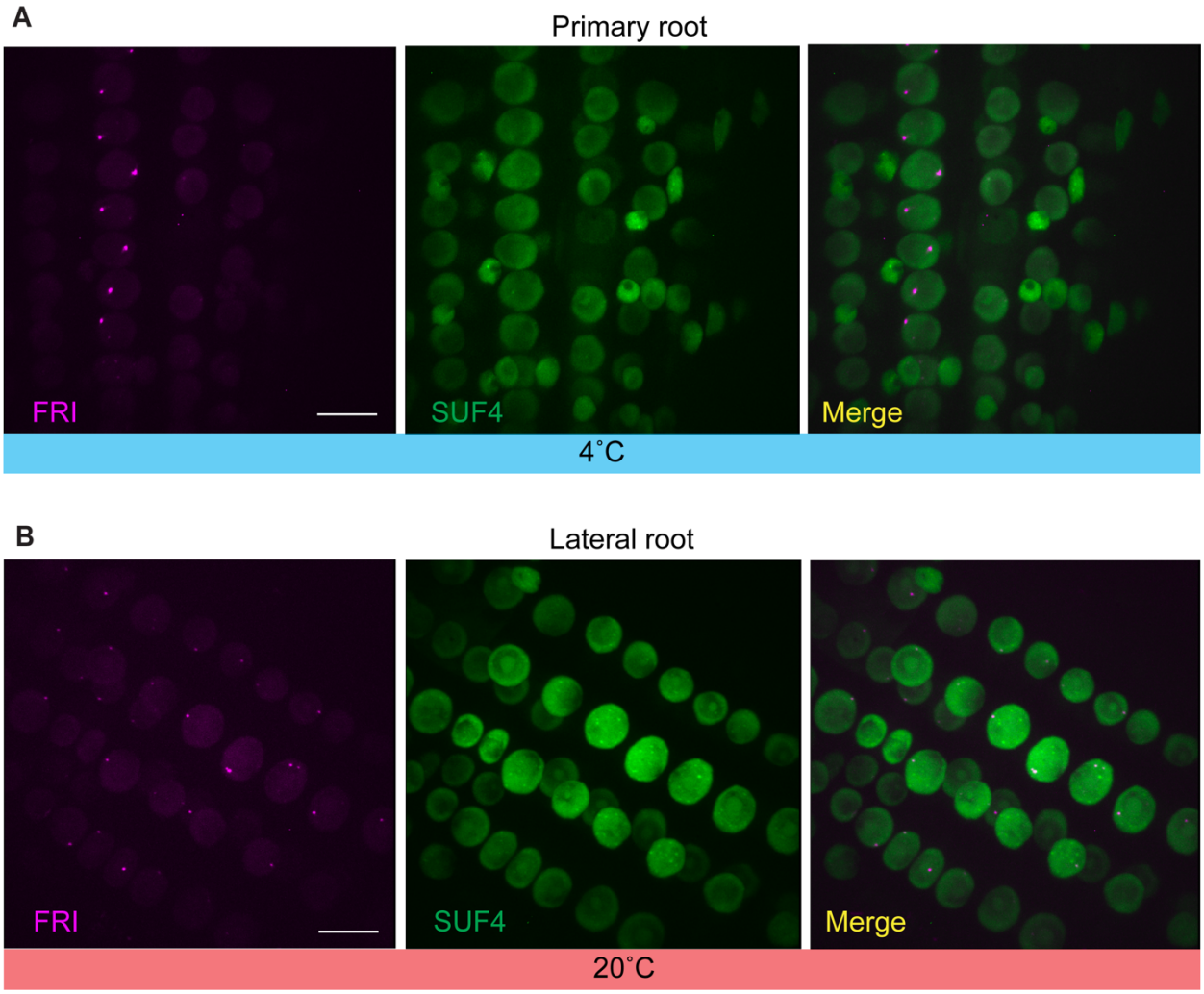

1212

1213 **Supplemental Figure 7. A)** FRI forms condensates in the primary root of 6 day
1214 old seedlings after 24 hours of 4˚C treatment. **B)** FRI forms condensates in a burst-
1215 like fashion in lateral roots under warm temperatures. Scalebars:10µm

1216
1217
1218
1219
1220
1221
1222

1223
1224
1225

Acknowledgements: We would like to thank Carlos Castañeda, Broder Schmidt, Adrienne Roeder, Rick Amasino, Doris Wagner, Ryan O'Hanlon, as well as the members of the Ehrhardt lab, IDPSIG, Carnegie Institution for Science, and Stanford University for their insightful comments and meaningful discussions.

Funding: H.M.M., T.H., Y.Z., and D.W.E. was supported on the Carnegie Venture Grant Fund. H.M.M. was also supported by the Simons Foundation-Life Science Research Foundation [Meyer LSRF18/Carnegie Fund 10861].

Author contributions:

Conceptualization: HMM, DWE, YZ

Methodology: HMM, DWE, YZ, TH, AM

Investigation: HMM, TH, DWE

Visualization: HMM, DWE

Funding acquisition: HMM, DWE, YZ

Supervision: DWE, YZ

Writing – original draft: HMM, DWE

Writing – review & editing: HMM, DWE, YZ

Competing interests: Authors declare that they have no competing interests

Data and materials availability: All data are available in the main text or the supplementary materials

1262 **REFERENCES:**

1263 1. Helliwell, C.A., Wood, C.C., Robertson, M., Peacock, W.J., and Dennis, E.S.
1264 (2006). The Arabidopsis FLC protein interacts directly in vivo with SOC1 and FT
1265 chromatin and is part of a high-molecular-weight protein complex. Plant J. *46*,
1266 183–192. 10.1111/j.1365-313x.2006.02686.x.

1267 2. Searle, I., He, Y., Turck, F., Vincent, C., Fornara, F., Kröber, S., Amasino, R.A.,
1268 and Coupland, G. (2006). The transcription factor FLC confers a flowering
1269 response to vernalization by repressing meristem competence and systemic
1270 signaling in Arabidopsis. Genes Dev. *20*, 898–912. 10.1101/gad.373506.

1271 3. Choi, K., Kim, J., Hwang, H.-J., Kim, S., Park, C., Kim, S.Y., and Lee, I.
1272 (2011). The FRIGIDA complex activates transcription of FLC, a strong flowering
1273 repressor in Arabidopsis, by recruiting chromatin modification factors. Plant cell
1274 *23*, 289–303. 10.1105/tpc.110.075911.

1275 4. Kim, S., Choi, K., Park, C., Hwang, H.-J., and Lee, I. (2006). SUPPRESSOR
1276 OF FRIGIDA4, Encoding a C2H2-Type Zinc Finger Protein, Represses Flowering
1277 by Transcriptional Activation of Arabidopsis FLOWERING LOCUS C. Plant Cell
1278 *18*, 2985–2998. 10.1105/tpc.106.045179.

1279 5. Csorba, T., Questa, J.I., Sun, Q., and Dean, C. (2014). Antisense COOLAIR
1280 mediates the coordinated switching of chromatin states at FLC during
1281 vernalization. Proc. Natl. Acad. Sci. *111*, 16160–16165.
1282 10.1073/pnas.1419030111.

1283 6. Kim, D.-H., and Sung, S. (2017). Vernalization-Triggered Intragenic Chromatin
1284 Loop Formation by Long Noncoding RNAs. Dev. Cell *40*, 302-312.e4.
1285 10.1016/j.devcel.2016.12.021.

1286 7. Kik, S.K., Christopher, D., Glauninger, H., Hickernell, C.W., Bard, J.A.M.,
1287 Ford, M., Sosnick, T.R., and Drummond, D.A. (2023). An adaptive biomolecular
1288 condensation response is conserved across environmentally divergent species.
1289 bioRxiv, 2023.07.28.551061. 10.1101/2023.07.28.551061.

1290 8. Moses, D., Ginell, G.M., Holehouse, A.S., and Sukenik, S. (2023). Intrinsically
1291 disordered regions are poised to act as sensors of cellular chemistry. Trends
1292 Biochem. Sci. *48*, 1019–1034. 10.1016/j.tibs.2023.08.001.

1293 9. Martin, E.W., and Mittag, T. (2018). Relationship of Sequence and Phase
1294 Separation in Protein Low-Complexity Regions. Biochemistry *57*, 2478–2487.
1295 10.1021/acs.biochem.8b00008.

1296 10. Jiang, H., Wang, S., Huang, Y., He, X., Cui, H., Zhu, X., and Zheng, Y.
1297 (2015). Phase Transition of Spindle-Associated Protein Regulate Spindle
1298 Apparatus Assembly. Cell *163*, 108–122. 10.1016/j.cell.2015.08.010.

1299 11. Wan, Y., Zheng, X., Chen, H., Guo, Y., Jiang, H., He, X., Zhu, X., and Zheng,
1300 Y. (2015). Splicing function of mitotic regulators links R-loop–mediated DNA
1301 damage to tumor cell killing. J Cell Biology *209*, 235–246.
1302 10.1083/jcb.201409073.

1303 12. Chin, A.F., Hilser, V.J., and Zheng, Y. (2019). The Disordered Protein Bugz
1304 Conserves Mitotic Function and Liquid-Liquid Phase Separation across 1.6 Billion
1305 Years of Evolution. Biophys J *116*, 179a–180a. 10.1016/j.bpj.2018.11.997.

1306 13. Stępiński, D. (2014). Functional ultrastructure of the plant nucleolus.
1307 Protoplasma *251*, 1285–1306. 10.1007/s00709-014-0648-6.

1308 14. Shaw, P.J., and Brown, J.W. (2004). Plant nuclear bodies. Curr. Opin. Plant
1309 Biol. *7*, 614–620. 10.1016/j.pbi.2004.09.011.

1310 15. Kalinina, N.O., Makarova, S., Makhotenko, A., Love, A.J., and Taliansky, M.
1311 (2018). The Multiple Functions of the Nucleolus in Plant Development, Disease
1312 and Stress Responses. Front. Plant Sci. *9*, 132. 10.3389/fpls.2018.00132.

1313 16. Rosa, S., Duncan, S., and Dean, C. (2016). Mutually exclusive sense–antisense
1314 transcription at FLC facilitates environmentally induced gene repression. Nat.
1315 Commun. *7*, 13031. 10.1038/ncomms13031.

1316 17. Ietswaart, R., Rosa, S., Wu, Z., Dean, C., and Howard, M. (2017). Cell-Size-
1317 Dependent Transcription of FLC and Its Antisense Long Non-coding RNA
1318 COOLAIR Explain Cell-to-Cell Expression Variation. Cell Syst. *4*, 622-635.e9.
1319 10.1016/j.cels.2017.05.010.

1320 18. Kroschwald, S., and Alberti, S. (2017). Gel or Die: Phase Separation as a
1321 Survival Strategy. Cell *168*, 947–948. 10.1016/j.cell.2017.02.029.

1322 19. Alberti, S. (2017). The wisdom of crowds: regulating cell function through
1323 condensed states of living matter. J. Cell Sci. *130*, 2789–2796. 10.1242/jcs.200295.

1324 20. Wang, Z., Lou, J., and Zhang, H. (2022). Essence determines phenomenon:
1325 Assaying the material properties of biological condensates. J. Biol. Chem. *298*,
1326 101782. 10.1016/j.jbc.2022.101782.

1327 21. Shin, Y., and Brangwynne, C.P. (2017). Liquid phase condensation in cell
1328 physiology and disease. Science *357*. 10.1126/science.aaf4382.

1329 22. Riback, J.A., Katanski, C.D., Kear-Scott, J.L., Pilipenko, E.V., Rojek, A.E.,
1330 Sosnick, T.R., and Drummond, D.A. (2017). Stress-Triggered Phase Separation Is
1331 an Adaptive, Evolutionarily Tuned Response. Cell *168*, 1028-1040.e19.
1332 10.1016/j.cell.2017.02.027.

1333 23. Vazquez, D.S., Toledo, P.L., Gianotti, A.R., and Ermácora, M.R. (2022).
1334 Protein conformation and biomolecular condensates. Curr. Res. Struct. Biol. *4*,
1335 285–307. 10.1016/j.crstbi.2022.09.004.

1336 24. Dorone, Y., Boeynaems, S., Flores, E., Jin, B., Hateley, S., Bossi, F., Lazarus,
1337 E., Pennington, J.G., Michiels, E., Decker, M.D., et al. (2021). A prion-like protein
1338 regulator of seed germination undergoes hydration-dependent phase separation.
1339 Cell *184*, 4284-4298.e27. 10.1016/j.cell.2021.06.009.

1340 25. Lasker, K., Boeynaems, S., Lam, V., Scholl, D., Stainton, E., Briner, A.,
1341 Jacquemyn, M., Daelemans, D., Deniz, A., Villa, E., et al. (2022). The material
1342 properties of a bacterial-derived biomolecular condensate tune biological function
1343 in natural and synthetic systems. Nat. Commun. *13*, 5643. 10.1038/s41467-022-
1344 33221-z.

1345 26. Zhu, P., Lister, C., and Dean, C. (2021). Cold-induced Arabidopsis FRIGIDA
1346 nuclear condensates for FLC repression. Nature *599*, 657–661. 10.1038/s41586-
1347 021-04062-5.

1348 27. Zhu, P., and Dean, C. (2023). Reply to: Cold induction of nuclear FRIGIDA
1349 condensation in Arabidopsis. Nature *619*, E33–E37. 10.1038/s41586-023-06190-6.

1350 28. Zhang, Z., Luo, X., Yang, Y., and He, Y. (2023). Cold induction of nuclear
1351 FRIGIDA condensation in Arabidopsis. Nature *619*, E27–E32. 10.1038/s41586-
1352 023-06189-z.

1353 29. Du, M., Stitzinger, S.H., Spille, J.-H., Cho, W.-K., Lee, C., Hijaz, M.,
1354 Quintana, A., and Cissé, I.I. (2024). Direct observation of a condensate effect on

1355 super-enhancer controlled gene bursting. Cell *187*, 331-344.e17.
1356 10.1016/j.cell.2023.12.005.

1357 30. Beckman, W.F., Jiménez, M.Á.L., and Verschure, P.J. (2021). Transcription
1358 bursting and epigenetic plasticity: an updated view. Epigenetics Commun. *1*, 6.
1359 10.1186/s43682-021-00007-1.

1360 31. Powers, S.K., Holehouse, A.S., Korasick, D.A., Schreiber, K.H., Clark, N.M.,
1361 Jing, H., Emenecker, R., Han, S., Tycksen, E., Hwang, I., et al. (2019). Nucleo-
1362 cytoplasmic Partitioning of ARF Proteins Controls Auxin Responses in
1363 Arabidopsis thaliana. Mol. Cell *76*, 177-190.e5. 10.1016/j.molcel.2019.06.044.

1364 32. Kim, S.Y., and Michaels, S.D. (2006). SUPPRESSOR OF FRI 4 encodes a
1365 nuclear-localized protein that is required for delayed flowering in winter-annual
1366 Arabidopsis. Development *133*, 4699–4707. 10.1242/dev.02684.

1367 33. He, Y., Doyle, M.R., and Amasino, R.M. (2004). PAF1-complex-mediated
1368 histone methylation of FLOWERING LOCUS C chromatin is required for the
1369 vernalization-responsive, winter-annual habit in Arabidopsis. Genes Dev. *18*,
1370 2774–2784. 10.1101/gad.1244504.

1371 34. Pazos, F., Pietrosemoli, N., García-Martín, J.A., and Solano, R. (2013). Protein
1372 intrinsic disorder in plants. Front. Plant Sci. *4*, 363. 10.3389/fpls.2013.00363.

1373 35. Bugge, K., Staby, L., Kemplen, K.R., O'Shea, C., Bendsen, S.K., Jensen,
1374 M.K., Olsen, J.G., Skriver, K., and Kragelund, B.B. (2018). Structure of Radical-
1375 Induced Cell Death1 Hub Domain Reveals a Common αα-Scaffold for Disorder in
1376 Transcriptional Networks. Structure *26*, 734-746.e7. 10.1016/j.str.2018.03.013.

1377 36. Jiang, J., Wang, T., Wu, Z., Wang, J., Zhang, C., Wang, H., Wang, Z.-X., and
1378 Wang, X. (2015). The Intrinsically Disordered Protein BKI1 Is Essential for
1379 Inhibiting BRI1 Signaling in Plants. Mol. Plant *8*, 1675–1678.
1380 10.1016/j.molp.2015.07.012.

1381 37. Shindo, C., Aranzana, M.J., Lister, C., Baxter, C., Nicholls, C., Nordborg, M.,
1382 and Dean, C. (2005). Role of FRIGIDA and FLOWERING LOCUS C in
1383 Determining Variation in Flowering Time of Arabidopsis. Plant Physiol. *138*,
1384 1163–1173. 10.1104/pp.105.061309.

1385 38. Fang, X., Wang, L., Ishikawa, R., Li, Y., Fiedler, M., Liu, F., Calder, G.,
1386 Rowan, B., Weigel, D., Li, P., et al. (2019). Arabidopsis FLL2 promotes liquid-

1387 liquid phase separation of polyadenylation complexes. Nature *569*, 265–269.
1388 10.1038/s41586-019-1165-8.

1389 39. Roberts, S., Harmon, T.S., Schaal, J.L., Miao, V., Li, K. (Jonathan), Hunt, A.,
1390 Wen, Y., Oas, T.G., Collier, J.H., Pappu, R.V., et al. (2018). Injectable tissue
1391 integrating networks from recombinant polypeptides with tunable order. Nat.
1392 Mater. *17*, 1154–1163. 10.1038/s41563-018-0182-6.

1393 40. Quiroz, F.G., and Chilkoti, A. (2015). Sequence heuristics to encode phase
1394 behaviour in intrinsically disordered protein polymers. Nat. Mater. *14*, 1164–1171.
1395 10.1038/nmat4418.

1396 41. Ruff, K.M., Roberts, S., Chilkoti, A., and Pappu, R.V. (2018). Advances in
1397 Understanding Stimulus-Responsive Phase Behavior of Intrinsically Disordered
1398 Protein Polymers. J. Mol. Biol. *430*, 4619–4635. 10.1016/j.jmb.2018.06.031.

1399 42. Dzuricky, M., Rogers, B.A., Shahid, A., Cremer, P.S., and Chilkoti, A. (2020).
1400 De novo engineering of intracellular condensates using artificial disordered
1401 proteins. Nat Chem *12*, 814–825. 10.1038/s41557-020-0511-7.

1402 43. Chen, J.W., Romero, P., Uversky, V.N., and Dunker, A.K. (2006).
1403 Conservation of Intrinsic Disorder in Protein Domains and Families: I. A Database
1404 of Conserved Predicted Disordered Regions. J. Proteome Res. *5*, 879–887.
1405 10.1021/pr060048x.

1406 44. Riley, A.C., Ashlock, D.A., and Graether, S.P. (2023). The difficulty of
1407 aligning intrinsically disordered protein sequences as assessed by conservation and
1408 phylogeny. PLOS ONE *18*, e0288388. 10.1371/journal.pone.0288388.

1409 45. Bao, Z., Zhang, N., and Hua, J. (2014). Endopolyploidization and flowering
1410 time are antagonistically regulated by checkpoint component MAD1 and immunity
1411 modulator MOS1. Nat Commun *5*, 5628. 10.1038/ncomms6628.

1412 46. Resentini, F., Cyprys, P., Steffen, J.G., Alter, S., Morandini, P., Mizzotti, C.,
1413 Lloyd, A., Drews, G.N., Dresselhaus, T., Colombo, L., et al. (2016).
1414 SUPPRESSOR OF FRIGIDA (SUF4) Supports Gamete Fusion via Regulating
1415 Arabidopsis EC1 Gene Expression. Plant Physiol. *173*, 155–166.
1416 10.1104/pp.16.01024.

1417 47. Leene, J.V., Hollunder, J., Eeckhout, D., Persiau, G., Slijke, E.V.D., Stals, H.,
1418 Isterdael, G.V., Verkest, A., Neirynck, S., Buffel, Y., et al. (2010). Targeted

1419 interactomics reveals a complex core cell cycle machinery in Arabidopsis thaliana.
1420 Mol. Syst. Biol. *6*, 397–397. 10.1038/msb.2010.53.

1421 48. Lee, I., and Amasino, R.M. (1995). Effect of Vernalization, Photoperiod, and
1422 Light Quality on the Flowering Phenotype of Arabidopsis Plants Containing the
1423 FRIGIDA Gene. Plant Physiol. *108*, 157–162. 10.1104/pp.108.1.157.

1424 49. Schindelin, J., Arganda-Carreras, I., Frise, E., Kaynig, V., Longair, M.,
1425 Pietzsch, T., Preibisch, S., Rueden, C., Saalfeld, S., Schmid, B., et al. (2012). Fiji:
1426 an open-source platform for biological-image analysis. Nat. Methods *9*, 676–682.
1427 10.1038/nmeth.2019.

1428 50. Thevenaz, P., Ruttimann, U.E., and Unser, M. (1998). A pyramid approach to
1429 subpixel registration based on intensity. IEEE Trans. Image Process. *7*, 27–41.
1430 10.1109/83.650848.

1431 51. Ershov, D., Phan, M.-S., Pylvänäinen, J.W., Rigaud, S.U., Blanc, L.L.,
1432 Charles-Orszag, A., Conway, J.R.W., Laine, R.F., Roy, N.H., Bonazzi, D., et al.
1433 (2022). TrackMate 7: integrating state-of-the-art segmentation algorithms into
1434 tracking pipelines. Nat. Methods *19*, 829–832. 10.1038/s41592-022-01507-1.

1435 52. Koulouras, G., Panagopoulos, A., Rapsomaniki, M.A., Giakoumakis, N.N.,
1436 Taraviras, S., and Lygerou, Z. (2018). EasyFRAP-web: a web-based tool for the
1437 analysis of fluorescence recovery after photobleaching data. Nucleic Acids Res.
1438 *46*, W467–W472. 10.1093/nar/gky508.

1439